













OPEN

# Large subglacial source of mercury from the southwestern margin of the Greenland Ice Sheet

Jon R. Hawkings<sup>1,2</sup>  , Benjamin S. Linhoff<sup>3,17</sup>, Jemma L. Wadham<sup>4,5</sup>, Marek Stibal<sup>6</sup> , Carl H. Lamborg<sup>7</sup>, Gregory T. Carling<sup>8</sup> , Guillaume Lamarche-Gagnon<sup>4</sup> , Tyler J. Kohler<sup>6,9</sup>, Rachael Ward<sup>4,10</sup>, Katharine R. Hendry<sup>10</sup> , Lukáš Falteisek<sup>6</sup>, Anne M. Kellerman<sup>1</sup>, Karen A. Cameron<sup>11</sup> , Jade E. Hatton<sup>6,10</sup>, Sarah Tingey<sup>4</sup>, Amy D. Holt<sup>1</sup>, Petra Vinšová<sup>6</sup> , Stefan Hofer<sup>12</sup> , Marie Bulínová<sup>6,13</sup>, Tomáš Větrovský<sup>14</sup>, Lorenz Meire<sup>15,16</sup>  and Robert G. M. Spencer<sup>1</sup>

**The Greenland Ice Sheet is currently not accounted for in Arctic mercury budgets, despite large and increasing annual runoff to the ocean and the socio-economic concerns of high mercury levels in Arctic organisms. Here we present concentrations of mercury in meltwaters from three glacial catchments on the southwestern margin of the Greenland Ice Sheet and evaluate the export of mercury to downstream fjords based on samples collected during summer ablation seasons. We show that concentrations of dissolved mercury are among the highest recorded in natural waters and mercury yields from these glacial catchments (521–3,300 mmol km<sup>-2</sup> year<sup>-1</sup>) are two orders of magnitude higher than from Arctic rivers (4–20 mmol km<sup>-2</sup> year<sup>-1</sup>). Fluxes of dissolved mercury from the southwestern region of Greenland are estimated to be globally significant (15.4–212 kmol year<sup>-1</sup>), accounting for about 10% of the estimated global riverine flux, and include export of bioaccumulating methylmercury (0.31–1.97 kmol year<sup>-1</sup>). High dissolved mercury concentrations (~20 pM inorganic mercury and ~2 pM methylmercury) were found to persist across salinity gradients of fjords. Mean particulate mercury concentrations were among the highest recorded in the literature (~51,000 pM), and dissolved mercury concentrations in runoff exceed reported surface snow and ice values. These results suggest a geological source of mercury at the ice sheet bed. The high concentrations of mercury and its large export to the downstream fjords have important implications for Arctic ecosystems, highlighting an urgent need to better understand mercury dynamics in ice sheet runoff under global warming.**

Mercury (Hg) is a toxic element of global concern with limited biological function. Hg bioaccumulates in organisms and biomagnifies in aquatic food webs largely as the neurotoxin methylmercury (MeHg, CH<sub>3</sub>Hg). Overexposure to Hg, primarily due to consumption of seafood, has major environmental and human health implications with a socio-economic cost estimated to exceed US \$5 billion per year<sup>1</sup>. The global Hg problem has worsened significantly due to anthropogenic pollution<sup>2,3</sup>, although there are natural sources of Hg to the environment such as volcanic emissions and weathering of Hg-bearing minerals in rock (for example, cinnabar)<sup>2</sup>. Hg is of particular concern in the Arctic<sup>1</sup>, where Hg concentrations in marine biota have increased by an order of magnitude over the past 150 years (ref. 4). This has led to health risks in local communities, where diets rely heavily on marine animals<sup>1</sup>. The Arctic is particularly vulnerable to anthropogenic Hg perturbations because it may be a global Hg sink as prevailing atmospheric circulation carries Hg to northern latitudes<sup>5</sup>. Although anthropogenic pollution is a major contributor to the elevated Hg concentrations in

Arctic biota, inputs from climatically vulnerable naturally occurring pools have also received more recognition during the last decade<sup>6–10</sup>. For example, Arctic rivers are a significant Hg source to the Arctic Ocean and are climatically sensitive due to their intensifying hydrological cycles (variability and magnitude), widespread catchment permafrost cover and disproportionate warming in the Arctic<sup>9,11</sup>. As yet, little consideration has been given to the Greenland Ice Sheet (GrIS) in the Arctic Hg cycle.

The GrIS is the second largest body of ice on Earth, covering nearly 25% of the land surface area in the Arctic region. Observed rapid and accelerating GrIS mass loss is producing increased annual freshwater runoff to coastal waters, which is predicted to nearly double in magnitude by 2100 (ref. 12). The biogeochemical implications of this increasing runoff are uncertain but likely important<sup>13,14</sup>. Only a handful of studies of Hg concentrations from Arctic proglacial rivers exist from the Canadian High Arctic Archipelago and disconnected glaciers (that is, those not part of the ice sheet) in east Greenland<sup>15–17</sup>, all showing moderate and climatically sensitive

<sup>1</sup>National High Magnetic Field Laboratory Geochemistry Group and Earth, Ocean, and Atmospheric Sciences, Florida State University, Tallahassee, FL, USA. <sup>2</sup>German Research Centre for Geosciences GFZ, Potsdam, Germany. <sup>3</sup>Woods Hole Oceanographic Institution, Woods Hole, MA, USA. <sup>4</sup>School of Geographical Sciences, University of Bristol, Bristol, UK. <sup>5</sup>Centre for Arctic Gas Hydrate, Environment and Climate (CAGE), Department of Geosciences, UiT The Arctic University of Norway, Tromsø, Norway. <sup>6</sup>Department of Ecology, Faculty of Science, Charles University, Prague, Czechia. <sup>7</sup>Department of Ocean Sciences, University of California, Santa Cruz, CA, USA. <sup>8</sup>Department of Geological Sciences, Brigham Young University, Provo, UT, USA. <sup>9</sup>Stream Biofilm and Ecosystem Research Laboratory, School of Architecture, Civil and Environmental Engineering, École Polytechnique Fédérale de Lausanne, Lausanne, Switzerland. <sup>10</sup>School of Earth Sciences, University of Bristol, Bristol, UK. <sup>11</sup>School of Geographical and Earth Sciences, University of Glasgow, Glasgow, UK. <sup>12</sup>Department of Geosciences, UiO University of Oslo, Oslo, Norway. <sup>13</sup>Department of Geosciences, UiT The Arctic University of Norway, Tromsø, Norway. <sup>14</sup>Laboratory of Environmental Microbiology, Institute of Microbiology of the Czech Academy of Sciences, Prague, Czechia. <sup>15</sup>Greenland Climate Research Centre, Greenland Institute of Natural Resources, Nuuk, Greenland. <sup>16</sup>Department of Estuarine and Delta Systems, Royal Netherlands Institute of Sea Research, Yerseke, the Netherlands. <sup>17</sup>Present address: US Geological Survey, Albuquerque, NM, USA. ✉e-mail: [jon.hawkings@gmail.com](mailto:jon.hawkings@gmail.com)

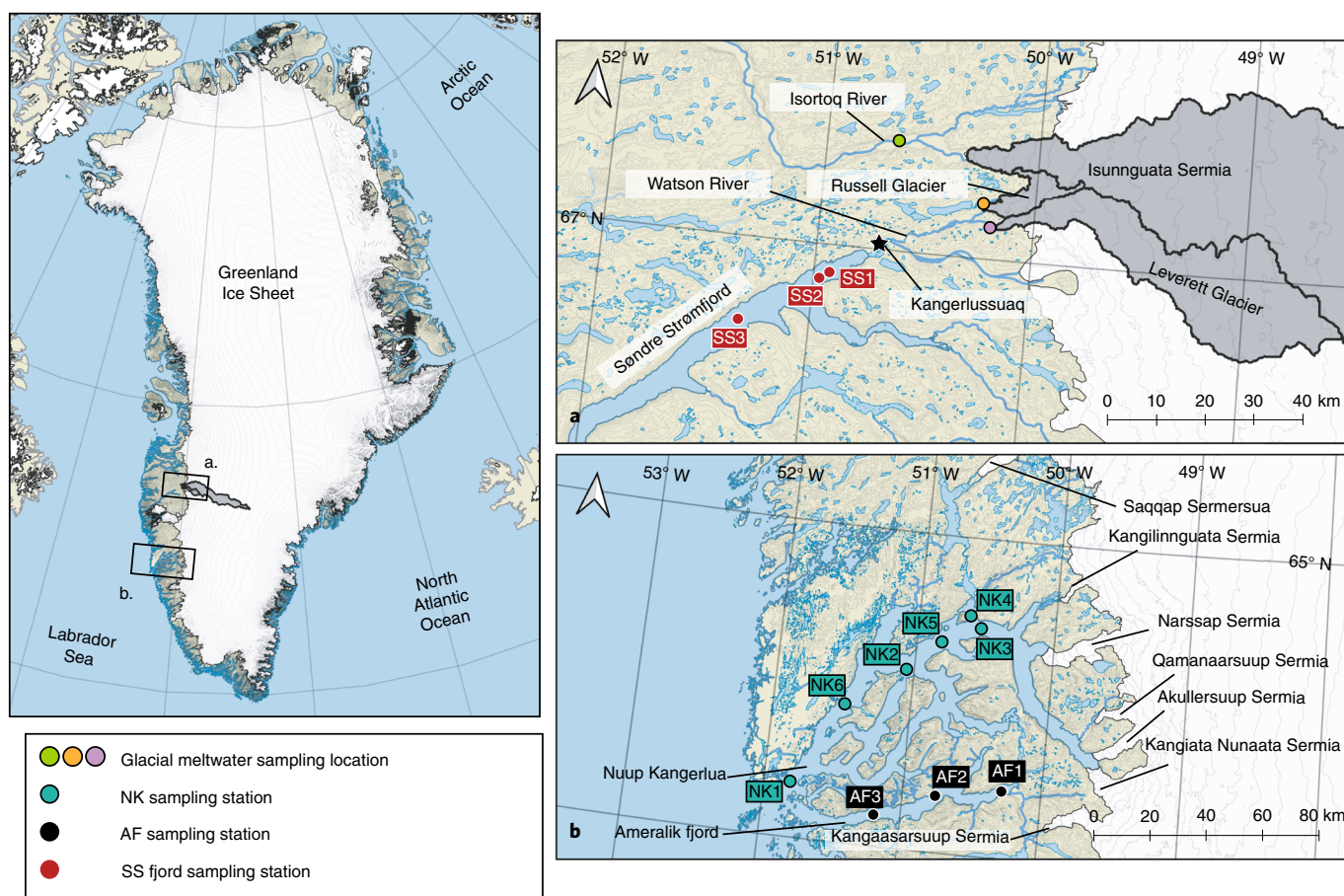


**Fig. 1 | Locations of sampling sites and stations.** **a, b**, Locations of riverine sampling sites (with modelled catchment areas in grey) and SS sampling stations (**a**), and NK and AF sampling stations (**b**). Field sites are indicated on the map of the GrIS (left) as **a** and **b**. Major glacial inputs into the NK and AF are indicated in **b**. Additional details can be found in the Methods.

Hg concentrations in glacial runoff. Glaciers in the Himalayas and Alaska have also been highlighted as Hg stores and sources to downstream ecosystems<sup>18–21</sup>, with all studies implying an atmospheric or ice-marginal Hg source. There are no data from runoff draining the large, polythermal-based catchments of the GrIS. Determining the role of the GrIS in the Arctic Hg cycle is therefore crucial in assessing Arctic ecosystem health both now and into the future.

Here, we evaluate Hg and MeHg concentrations in meltwaters originating from the southwestern margin of the GrIS and export to downstream fjords (Fig. 1). The study focuses on a >4,000 km<sup>2</sup> region of the GrIS that covers three glacial catchments ranging from ~85 to 3,200 km<sup>2</sup> in size (Russell Glacier (RG), Leverett Glacier (LG) and Isunnguata Sermia (IS)), and three fjord systems (Nuup Kangerlua (NK), Ameralik Fjord (AF) and Søndre Strømfjord (SS)), which receive substantial GrIS meltwater inputs (Fig. 1 and Methods). All GrIS catchments sampled are warm based from the ice sheet margin and have well-developed subglacial hydrological systems, likely with regions of anoxia<sup>22,23</sup>. Data are presented for total Hg (THg), particulate Hg (pHg, >0.45 μm), total dissolved Hg (dHg, <0.45 μm), size-fractionated dissolved Hg (cHg = 0.02–0.45 μm, sHg = <0.02 μm), dissolved inorganic Hg<sup>2+</sup> (dIHg, <0.45 μm) and dissolved methylmercury (dMeHg, <0.45 μm) over four field seasons. Complementary metagenomic sequencing of DNA from the subglacial microbial community sampled from subglacial meltwaters exiting LG is used to hypothesize Hg biogeochemical pathways through the identification of *hgcAB*, *merA* and *merB* genes. Our results provide evidence for the importance of ice sheet runoff in

regional Hg cycling and indicate that coastal Hg dynamics are likely to change under climatic warming scenarios.

### Mercury concentrations and speciation in meltwater rivers

Measurements of Hg in GrIS subglacial runoff over all sampling periods and sites were similar to contaminated and urban watersheds but much higher than those reported for glacierized and non-glacierized environments elsewhere (Table 1 and Supplementary Table 1)<sup>28</sup>. High concentrations of dHg were observed in samples of runoff taken through June and July 2018 across three GrIS catchments (Fig. 2 and Table 1). Discharge-weighted mean concentrations of dIHg (Hg<sup>0</sup> + Hg<sup>2+</sup>) were 603–1,260 pM (LOADEST modelled mean concentrations were 607–1,310 pM; Supplementary Table 2). There appear to be systematic differences in the dIHg concentrations observed between glacial catchments that may be explained by underlying bedrock type (Extended Data Fig. 1). Two of the glaciers (IS and RG) located predominantly on the Nagsstugtoqidian mobile belt have significantly lower ( $P < 0.05$ ;  $n = 28$ ) dIHg concentrations (mean 632 and 603 pM, respectively) than LG, which predominantly overlies an Archaean block geological belt to the south (1,260 pM; Extended Data Fig. 1). The larger glacial catchments (LG and IS) show a gradually increasing trend in dIHg over time ( $R^2 = 0.20$  ( $P < 0.15$ ;  $n = 12$ ) and 0.54 ( $P < 0.05$ ;  $n = 14$ ), respectively), concurrent with increasing discharge and seasonal subglacial hydrological system expansion (Fig. 2). The smallest catchment (RG) displays relatively invariant dIHg concentrations and discharge during the observation period (Fig. 2). Meltwater

**Table 1 | Measured discharge-weighted mean concentrations, estimated fluxes and estimated yields of dissolved mercury species**

Study area	Catchment size km <sup>2</sup>	Discharge km <sup>3</sup> year <sup>-1</sup>	Concentration			Estimated flux			Estimated yield			Source
			dIHg	dMeHg	dHg	dIHg	dMeHg	dHg	dIHg	dMeHg	dHg	
			pM <sup>a</sup>			kmol year <sup>-1</sup>			mmol km <sup>-2</sup> year <sup>-1</sup>			
LG	850	1.5 <sup>b</sup>	1260 (627–1,730)	8.8 (5.79–13.7)	1,270 (633–1,740)	1.89 (0.95–2.59)	0.01 (0.01–0.02)	1.90 (0.96–2.61)	2,220 (1,110–3,050)	15.5 (10.2–24.2)	2,230 (1,120–3,080)	This study
RG	85	0.31 <sup>c</sup>	632 (451–889)	12.9 (10.8–16.2)	645 (462–905)	0.20 (0.14–0.28)	0.004 (0.003–0.01)	0.20 (0.14–0.28)	2,300 (1,640–3,240)	47.0 (39.4–59.1)	2,350 (1,680–3,300)	This study
IS	3,200	7.6 <sup>c</sup>	603 (215–970)	7.6 (4.5–10.5)	611 (220–981)	4.58 (1.63–7.37)	0.06 (0.03–0.08)	4.64 (1.67–7.45)	1,430 (511–2,300)	18.1 (10.7–24.9)	1,450 (521–2,330)	This study
GrIS– southwestern margin	230,000	122 <sup>a</sup>	720 <sup>d</sup> (215–1,730)	8.1 <sup>d</sup> (4.47–16.2)	728 <sup>d</sup> (219–1,750)	87.8 (15.1–210)	0.99 (0.31–1.97)	88.8 (15.4–212)	382 (65.6–915)	4.3 (1.36–8.56)	386 (67.0–923)	This study
Arctic rivers <sup>f</sup>		3,500		1.4–3.7 <sup>e</sup>	28–74 <sup>f</sup>		9.2 <sup>e</sup>	184 <sup>f</sup>		0.2–1.0 <sup>e</sup>	4.0–19.9 <sup>f</sup>	Ref. <sup>9</sup>
Global rivers		37,000		1.18 <sup>e</sup>	23.5 (0.5–3,000)		43.5 <sup>g</sup>	870 (580–1,160)				Ref. <sup>8</sup>

Upscaled preliminary estimates for the southwestern region of the GrIS (Extended Data Fig. 3) are based calculated from the discharge-weighted mean value from the three glacial catchments. Estimates from Arctic rivers and a global river range are given for comparison. A range of estimates are given in parentheses and are derived from the minimum and maximum concentrations recorded at each field site or the sample set (for GrIS southwestern margin). Values from this study are presented to three significant figures or two decimal places. LOADEST estimates are provided in Supplementary Table 2. <sup>a</sup>Mean concentrations from glacial catchments are discharge-weighted mean concentrations. <sup>b</sup>2009–2012, 2015<sup>33,49</sup>. <sup>c</sup>Modelled 2009–2018 MAR catchment runoff<sup>50</sup>. <sup>d</sup>Discharge-weighted mean concentration from all LG, RG and IS Hg samples (see Methods). <sup>e</sup>Mean modelled MAR southwestern GrIS meltwater discharge from 2009 to 2018<sup>50</sup>. Catchment area includes ice sheet surface up to the ice divide (that is, regions that are not hydrologically active; Extended Data Fig. 3). Minimum is the lowest discharge year (2009); maximum is the largest discharge year (2012). <sup>f</sup>Hg concentrations, fluxes and yields. <sup>g</sup>Estimated assuming ~5% of dHg is MeHg, which is an upper end estimate from the Mackenzie River<sup>10</sup>.

dIHg concentrations reported here are one to two orders of magnitude greater than dHg concentrations in Arctic rivers (1.5–14 pM; Supplementary Table 1), and more than an order of magnitude higher than Arctic river THg concentrations (28–74 pM; Table 1). The differences between GrIS meltwaters and Arctic rivers are also reflected in extremely high dIHg catchment yields (1,440–2,310 mmol km<sup>-2</sup> year<sup>-1</sup>; Table 1), approximately two orders of magnitude higher than large Arctic rivers (4–20 mmol km<sup>-2</sup> year<sup>-1</sup>). Only polluted rivers and estuaries in Asia have been shown to have similar or higher concentrations of dIHg (up to 50,000 pM; Supplementary Table 1)<sup>24,25</sup>.

Methylmercury concentrations from the three catchments (Fig. 2d) indicate substantial export of bioavailable Hg and potential Hg cycling pathways in subglacial ecosystems. Concentrations of dMeHg are relatively high from all three glacial catchments (>5 pM), exceeding values from most pristine freshwaters, and similar to those found in wetlands (below detection in rivers to 2.5 pM in the Everglades)<sup>2,16,26</sup>. Dissolved dMeHg accounts for 0.74 ± 0.17% (LG), 1.5 ± 0.97% (IS) and 2.1 ± 0.43% (RG) of the total dHg concentration, which is in the range of other freshwater systems (~1–10%)<sup>2</sup>, including Arctic rivers (~0.2–5%)<sup>10</sup>, but lower than marine environments (4–22%)<sup>27</sup>. The higher concentrations of dMeHg in RG outflow coincide with higher mean dissolved organic carbon (DOC) concentrations compared with LG and IS (16 ± 2 μM versus 12 ± 4 μM, respectively; Extended Data Fig. 2), and higher methane (CH<sub>4</sub>) concentrations compared with LG<sup>23,28</sup>. These differences suggest that variations in subglacial hydrology and/or organic matter content and supply beneath each catchment are important for dMeHg cycling. In addition, a greater fraction of meltwaters may originate from hypoxic/anoxic regions of the glacier bed at RG (hypothesized due to the high CH<sub>4</sub> concentrations<sup>22,29</sup>) where potential for methylation is higher<sup>1,30</sup>. There may also be an influence of river-marginal inputs in the RG catchment (for example, proglacial lakes and tundra) given that the meltwater river travels along the ice margin for ~9 km before arriving at the sampling site. High concentrations of dMeHg in the glacial catchments sampled here therefore point to spatially heterogeneous subglacial water sources and hydrological flow pathways, a psychrophilic mercury cycling

microbial community capable of mercury cycling and/or abiotic dIHg methylation<sup>23,31</sup>. The dMeHg concentrations also have detrimental implications for bioaccumulation of ice sheet-derived Hg in Arctic ecosystems. Collectively, the Hg concentrations here lead to first-order estimates of dHg fluxes from the southwestern region of the GrIS (Extended Data Fig. 3) of 87.8 (15.1–210) kmol year<sup>-1</sup> dIHg and 0.99 (0.31–1.97) kmol year<sup>-1</sup> dMeHg (Table 1), which are within the same order of magnitude as Arctic rivers and with much higher yields (382 mmol km<sup>-2</sup> year<sup>-1</sup> dIHg and 4.3 mmol km<sup>-2</sup> year<sup>-1</sup> dMeHg; Table 1), highlighting the importance of previously unquantified ice sheet runoff in the Arctic Hg cycle.

A 2015 time series dataset from May to the end of July from LG (Fig. 3) indicates temporal variability and distinctive size fractionation in dHg. Concentrations followed the seasonal hydrological drainage evolution of LG and are divided into four time periods<sup>22,32</sup> (Fig. 3): (1) lower concentrations during the initial onset of melt in early May (day 135–150), (2) opening of the subglacial portal (day 152)<sup>22</sup> corresponding to sHg increasing from ~1,800 pM to ~4,200 pM, (3) the ‘outburst’ period, where the subglacial hydrological system was perturbed by water inputs from supraglacial meltwater drainage events<sup>22,33</sup> (day 170–190; 1,000–5,000 pM sHg and 2,000–18,000 pM cHg) and (4) the post-outburst period (day 190 onward), where discharge was largely controlled by the intensity of surface melt and Hg concentrations fell to a seasonal minimum before increasing, with the decline in discharge observed around day 208 (Fig. 3). There appeared to be a weak relationship between outburst events and Hg concentration. For example, sHg was elevated during outburst events 1, 2 and 4 (blue regions in Fig. 3) compared with immediately before, similar to trends observed in CH<sub>4</sub> and DOC (refs. <sup>22,32</sup>), indicating periodic flushing of isolated subglacial waters high in Hg. A rise in Hg concentrations during a period of decreasing discharge in period 4 reinforces a previous hypothesis that lower subglacial water pressure in subglacial channels as discharge falls results in drainage of concentrated channel-marginal waters from more isolated regions of the subglacial environment into main drainage channels along a hydraulic gradient<sup>23,33</sup>. Total dHg was dominated by cHg species (0.02–0.45 μm; mean 82% of

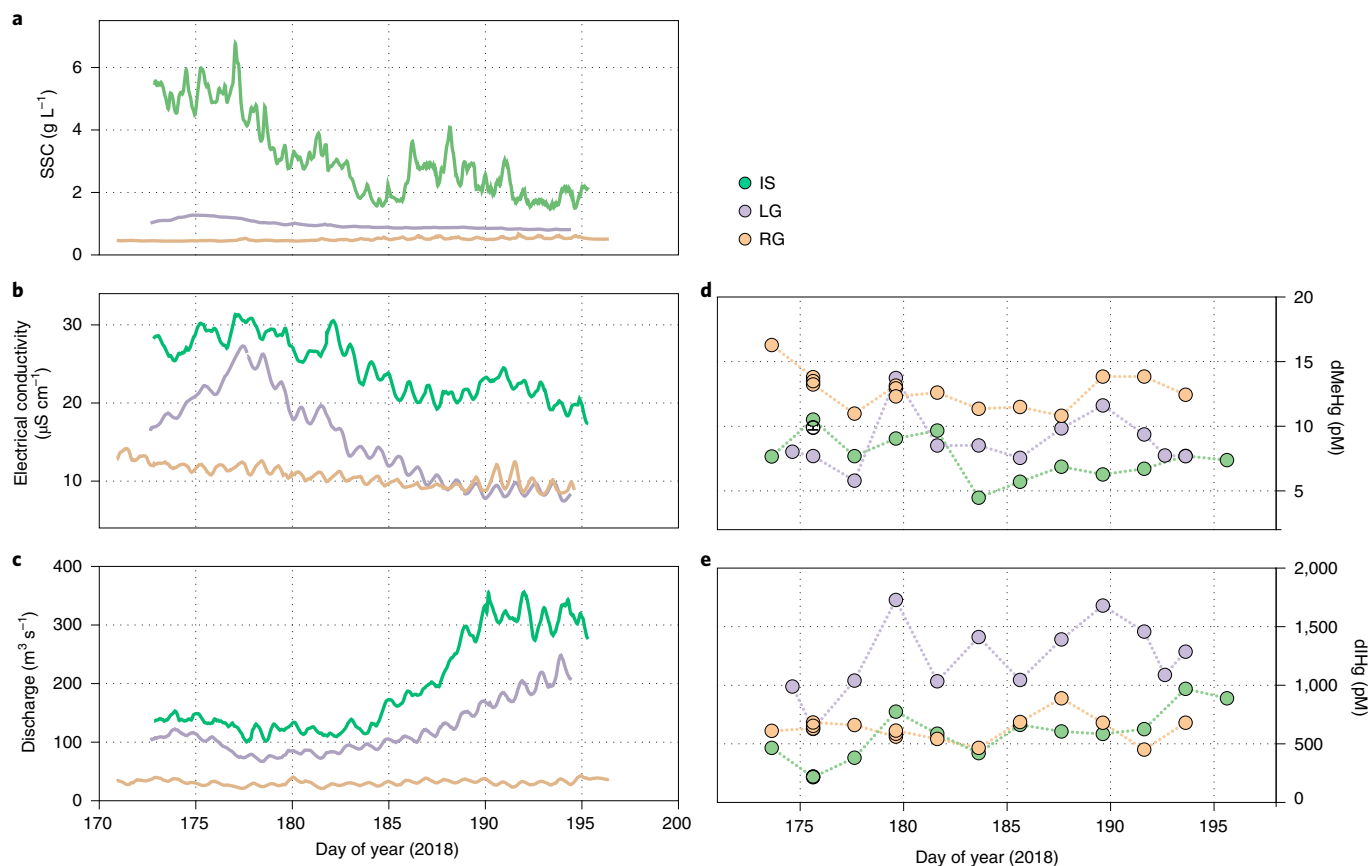


**Fig. 2 | Concurrent hydrogeochemical time series of LG, IS and RG proglacial rivers in June–July 2018. a–e,** Suspended sediment concentration (SSC) (**a**), electrical conductivity (**b**), discharge (**c**), dissolved methylmercury (dMeHg,  $<0.45 \mu\text{m}$ ) concentrations (**d**) and dissolved inorganic mercury concentrations (dIHg,  $<0.45 \mu\text{m}$ ) (**e**).

dHg), similar to other trace elements in ice sheet meltwaters<sup>34</sup>. High colloidal Fe and Al concentrations ( $>1 \mu\text{M}$ )<sup>34</sup> indicate cHg species are likely adsorbed to inorganic nanoparticle minerals (for example, Fe and Al (oxy)hydroxides).

### Mercury cycling genes in the subglacial microbiome

DNA metagenomic analysis from LG meltwater suggests that subglacial microbial communities are genetically equipped to deal with Hg, consistent with other Arctic environments<sup>35</sup>. Microbes have been shown to cope with  $\text{Hg}^{2+}$  toxicity by transforming it into volatile  $\text{Hg}^0$  using mercuric reductase encoded by the *merA* gene and respond to MeHg stress by using the organomercurial lyase encoded by the *merB* gene to de-methylate MeHg into  $\text{Hg}^0$  (and  $\text{CH}_4$ )<sup>36,37</sup>. Analysis of the microbial metagenomes at LG during 2015 showed the presence of *merA* and *merB* genes (Extended Data Fig. 4 displays taxa bearing the *merA* gene, a subset of which also carry the *merB* gene), while genes encoding for known Hg methylation (*hgcAB*)<sup>38</sup> were not detected. The presence of dMeHg and absence of *hgcAB* has also been reported for marine environments<sup>37</sup>, indicating that other poorly described microorganisms and metabolic pathways may be important for Hg methylation, or that abiotic methylation predominates<sup>31</sup>. Clearly, there is a need to better constrain the activity of Hg cycling microbes in subglacial environments and their impact on the speciation of exported Hg.

### Environmentally high mercury concentrations in fjords

Hg concentrations in Greenlandic fjords help elucidate whether inputs from glacial meltwaters have the potential to impact downstream ecosystem health. We find that environmentally high surface

dIHg and dMeHg concentrations are sustained downstream of glacial inputs in NK and AF in a region with bedrock geology similar to the Kangerlussuaq field sites (Figs. 1 and 4 and Supplementary Table 1). Surface concentrations of dIHg ranged from 12.5 to 30.6 pM (Fig. 4a). Lower values were measured at higher salinities, consistent with seawater dilution of a glacial meltwater Hg source. At the salinities sampled in these fjord systems (17.0–32.4), dIHg appears to mix linearly (Fig. 4a;  $R^2 = 0.70$  ( $P < 0.05$ ;  $n = 9$ )) with lower concentrations at higher salinities implying seawater dilution, but this does not follow a two end-member mixing model using the data from the northern ice sheet catchments sampled. We hypothesize non-conservative behaviour at lower salinities due to removal of Hg by scavenging on flocculated particles, alongside biological and/or photochemical reduction of  $\text{Hg}^{2+}$  to  $\text{Hg}^0$  with subsequent degassing<sup>26</sup>, which is implied by a more limited dataset from SS (Fig. 1) downstream of RG and LG inputs (see the dHg concentrations from fjord waters with salinity 0.4–8.3 in Extended Data Fig. 5).

Dissolved methylmercury (dMeHg) in fjord surface waters accounted for a larger proportion of dHg than meltwater runoff (6–14% versus 0.6–4.7%), and the percentage composition was positively correlated with salinity ( $R^2 = 0.49$ ;  $P < 0.05$ ;  $n = 9$ ), consistent with trends observed in marine environments elsewhere<sup>27</sup>. The dMeHg concentrations were slightly lower than those found in meltwaters (1.56–2.59 pM versus 4.47–16.2 pM), but much higher than open ocean concentrations (0.02–0.13 pM)<sup>27</sup>, indicating non-conservative mixing and dMeHg enhancement in the fjord (Fig. 4b). Additional inputs may include microbial methylation in the water column or fjord sediments, which are likely to be anoxic<sup>39</sup>. The dIHg and MeHg concentrations were more than an

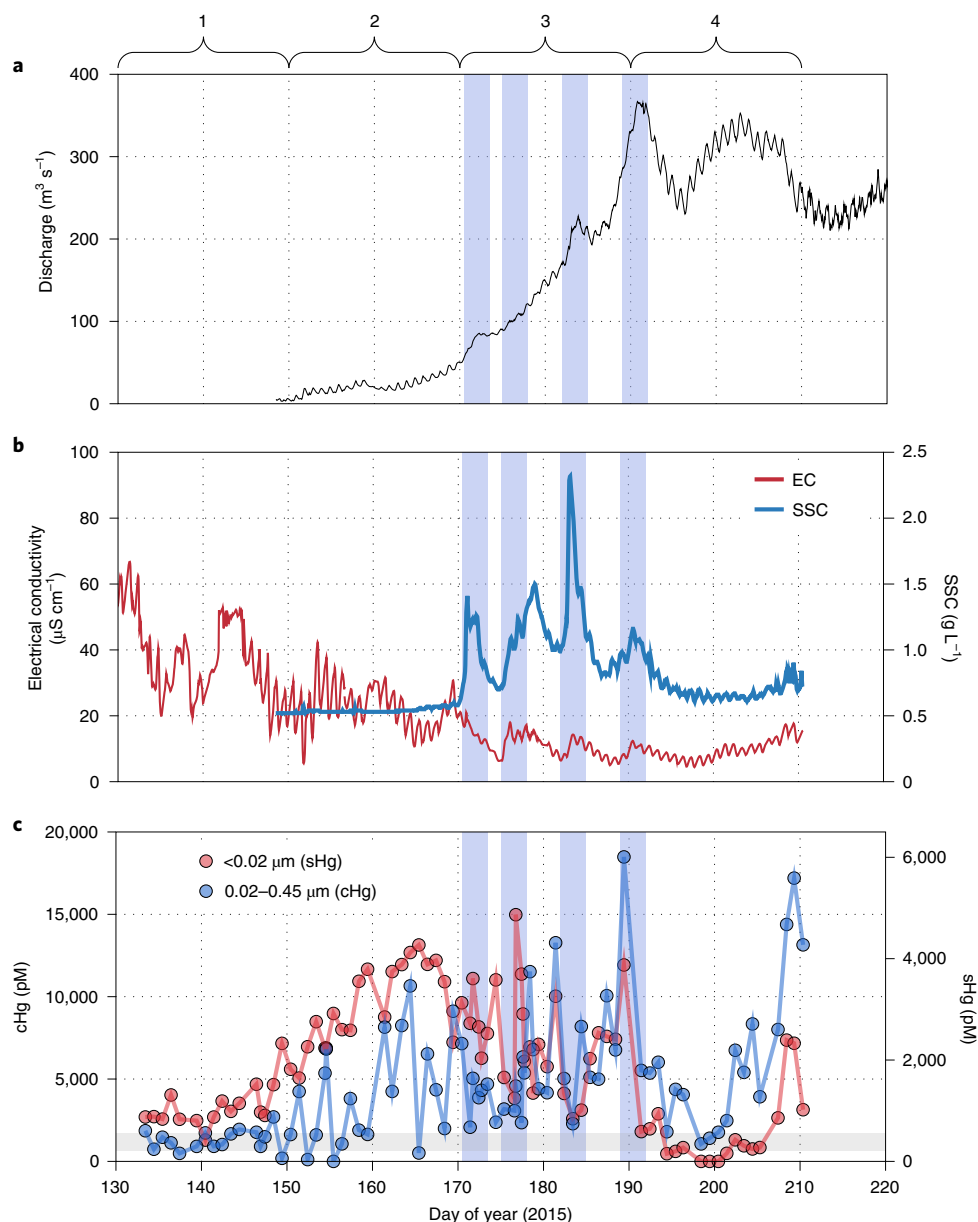


**Fig. 3 | Hydrogeochemical and metagenomic time series of LG proglacial river in 2015. a–c,** Meltwater discharge (**a**), electrical conductivity and suspended sediment concentration (SSC) (**b**) and soluble (sHg,  $<0.02\ \mu\text{m}$ ) and colloidal/nanoparticulate mercury (cHg,  $0.02\text{--}0.45\ \mu\text{m}$ ) (**c**) concentrations. Shaded blue regions indicate outburst event periods, corresponding to abrupt changes in EC, SSC and discharge due to supraglacial meltwater entering the subglacial hydrological system and forcing stored waters from the ice sheet bed. Four Hg concentration time periods are indicated above **a**.

order of magnitude higher than values reported for the upper water column in major ocean basins (THg  $0.19\text{--}1.3\ \text{pM}$ , MeHg  $0.02\text{--}0.13\ \text{pM}$ )<sup>27</sup>, including the proximal Labrador Sea (THg  $0.25\text{--}0.66\ \text{pM}$ , MeHg  $0.03\text{--}0.12\ \text{pM}$ )<sup>40,41</sup>. These data therefore highlight a role for Greenlandic fjords as Hg hotspots and demonstrate the potential importance of local Hg sources to coastal Arctic ecosystems.

#### Likely source of mercury to ice sheet meltwaters

The precise origin of Hg in GrIS meltwaters is unknown. The majority of Hg delivered by GrIS meltwater runoff is unlikely to come from anthropogenically derived atmospheric Hg deposited on the ice sheet surface and transported through surface melt because dHg concentrations in meltwater rivers exceed all reported surface snow and ice values ( $<0.3\text{--}150\ \text{pM}$ )<sup>18</sup>, including samples from the GrIS ( $<0.3\text{--}10\ \text{pM}$ )<sup>42</sup>. Additionally, a large proportion of supraglacial Hg is likely to be photochemically reduced to  $\text{Hg}^0$  and volatilized under

the high-irradiance conditions<sup>18</sup>. Evidence of high Hg in the subglacial environment of the southwestern sector of the GrIS comes from pHg concentrations measured at LG, which are expected to integrate the bedrock/sediment signal of the hydrologically active catchment. The pHg concentrations in LG suspended sediment range from  $\sim 8.5$  to  $>90\ \text{nmol g}^{-1}$  (mean  $44\ \text{nmol g}^{-1}$ ), which, with the elevated suspended sediment concentrations found in Greenlandic meltwaters ( $\sim 1\ \text{g L}^{-1}$ ; Figs. 2a and 3a), correspond to very high pHg concentrations of  $11\text{--}73\ \text{nM}$  (Supplementary Table 1). Particulate Hg concentrations represent the higher limit of previously measured samples and are comparable only to igneous/metamorphosed rock and lake sediment concentrations in Hg-rich geological deposits, including sediment samples overlying Precambrian shield bedrock in Canada (up to  $105\ \text{nmol g}^{-1}$ )<sup>2,43,44</sup>. These findings are unexpected and imply a poorly understood mechanism of Hg enrichment, the existence of relatively large quantities of Hg-bearing minerals such as cinnabar

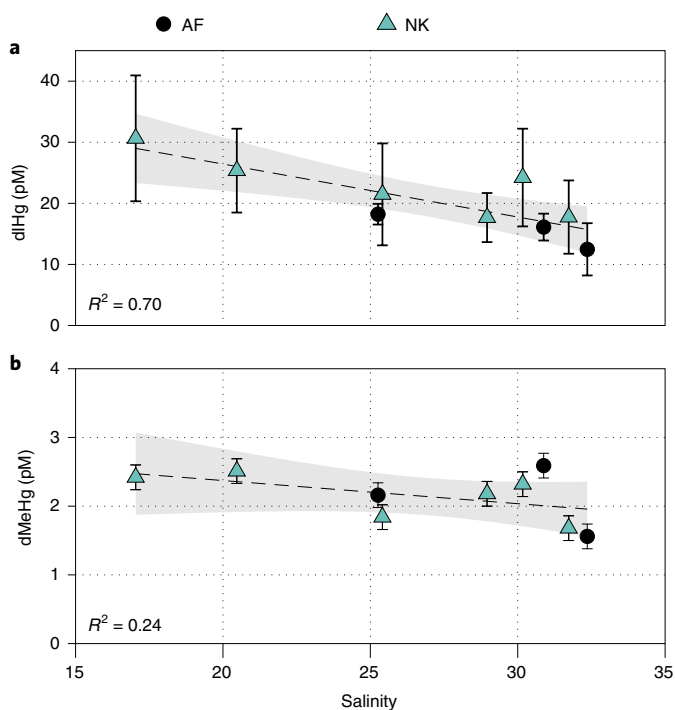


**Fig. 4 | NK and AF surface dissolved mercury concentrations over salinity gradients. a,b.** Dissolved inorganic mercury (dIHg) (**a**) and dissolved methylmercury (dMeHg) (**b**) concentrations. Error bars reflect either instrumental precision (dMeHg) or the standard deviation of measurements between three Hg laboratories (dIHg). An approximate conservative mixing line is given, assuming that freshwater end members in these fjords have Hg concentrations similar to meltwaters sampled in the Kangerlussuaq area, and using values from the Labrador Sea as a high-salinity end member<sup>40,41</sup>. Linear regressions of dMeHg/dIHg concentrations against salinity are given with corresponding  $R^2$  values. Shaded grey regions indicate 95% confidence bounds on the linear regressions.

in subglacial sediments and/or the influence of overridden Hg-rich permafrost that is being gradually eroded. Overridden permafrost is an unlikely source because pHg concentrations would have to vastly exceed those recorded in recent studies ( $0.06\text{--}0.4\text{ nmol g}^{-1}$ )<sup>11</sup>. Instead the unique physicochemical properties of glacial environments are likely to enhance mobilization of Hg in Hg-rich bedrock because of intense bedrock comminution by physical erosion that produces an abundance of freshly weathered microparticles<sup>15</sup>. There is also evidence of geothermal activity under large portions of the GrIS (refs. <sup>46–48</sup>), potentially manifested locally at LG by an iron-rich groundwater spring located 400 m in front of the glacial terminus<sup>46</sup> with a sHg concentration  $>20,000\text{ pM}$ . This geothermal activity may be associated with the presence of the geological divide between the Nagsugtoqidian mobile belt to the north and the Archaean block to the south and/or geothermal hotspots under southwestern and central Greenland<sup>46,47</sup> (Extended Data Fig. 1).

Data collected from meltwater rivers draining a  $\sim 4000\text{ km}^2$  region of the GrIS and two fjords receiving meltwater runoff indicate a large export of Hg from southwestern Greenland. Extremely high Hg yields, coupled with dMeHg concentrations of environmental concern, highlight the need to better understand ice sheet processes in the Hg cycle, especially the elevated pHg concentrations, which likely fuel the ice sheet Hg cycle. Hypothesized microbial cycling of Hg in the subglacial environment, including unidentified methylation pathways and as a mechanism of protection from the high levels of dissolved inorganic Hg present, provides additional support for the importance of Hg in these systems, but additional evidence

is still needed to demonstrate activity of the *merA* and *merB* metabolic pathways. Our data indicate that glacial meltwater-sourced Hg impacts downstream fjords, where much lower but environmentally high concentrations persist, with high potential for Hg bioaccumulation in coastal food webs. It is highly uncertain how projected increases in ice sheet melt rates due to climatic warming in the Arctic will impact Hg export; however, we postulate that rising meltwater runoff will increase Hg yields and therefore downstream flux. This large, unaccounted for and climatically sensitive Hg source has not been considered in current global Hg budgets and Hg management strategies, but it should be assessed urgently given the human and economic implications of elevated Hg exposure.

### Online content

Any methods, additional references, Nature Research reporting summaries, source data, extended data, supplementary information, acknowledgements, peer review information; details of author contributions and competing interests; and statements of data and code availability are available at <https://doi.org/10.1038/s41561-021-00753-w>.

Received: 11 March 2021; Accepted: 8 April 2021;  
Published online: 24 May 2021

### References

- Lehnher, I. Methylmercury biogeochemistry: a review with special reference to Arctic aquatic ecosystems. *Environ. Rev.* **22**, 229–243 (2014).
- Fitzgerald, W. F. & Lamborg, C. H. in *Treatise on Geochemistry* 2nd ed (eds Holland, H. D. & Turekian, K. K.) 91–129 (Elsevier, 2014).
- Lamborg, C. et al. Mercury in the Anthropocene Ocean. *Oceanography* **27**, 76–87 (2014).
- Dietz, R., Outridge, P. M. & Hobson, K. A. Anthropogenic contributions to mercury levels in present-day Arctic animals—A review. *Sci. Total Environ.* **407**, 6120–6131 (2009).
- Steffen, A., Schroeder, W., Macdonald, R., Poissant, L. & Konoplev, A. Mercury in the Arctic atmosphere: an analysis of eight years of measurements of GEM at Alert (Canada) and a comparison with observations at Amderma (Russia) and Kuujjuarapik (Canada). *Sci. Total Environ.* **342**, 185–198 (2005).
- Fisher, J. A. et al. Riverine source of Arctic ocean mercury inferred from atmospheric observations. *Nat. Geosci.* **5**, 499–504 (2012).
- Zhang, Y. et al. Biogeochemical drivers of the fate of riverine mercury discharged to the global and Arctic oceans. *Glob. Biogeochem. Cycles* **29**, 854–864 (2015).
- Amos, H. M. et al. Global biogeochemical implications of mercury discharges from rivers and sediment burial. *Environ. Sci. Technol.* **48**, 9514–9522 (2014).
- Zolkos, S. et al. Mercury export from Arctic great rivers. *Environ. Sci. Technol.* **54**, 4140–4148 (2020).
- Emmerton, C. A. et al. Mercury export to the Arctic Ocean from the Mackenzie River, Canada. *Environ. Sci. Technol.* **47**, 7644–7654 (2013).
- Schuster, P. F. et al. Permafrost stores a globally significant amount of mercury. *Geophys. Res. Lett.* **45**, 1463–1471 (2018).
- Muntjewerf, L. et al. Greenland Ice Sheet contribution to 21st century sea level rise as simulated by the coupled CESM2.1–CISM2.1. *Geophys. Res. Lett.* **47**, e2019GL086836 (2020).
- Wadham, J. L. et al. Ice sheets matter for the global carbon cycle. *Nat. Commun.* **10**, 3567–3567 (2019).
- Hopwood, M. J. et al. Review article: how does glacier discharge affect marine biogeochemistry and primary production in the Arctic? *Cryosphere* **14**, 1347–1383 (2020).
- Søndergaard, J. et al. Mercury exports from a high-Arctic river basin in northeast Greenland ( $74^\circ\text{N}$ ) largely controlled by glacial lake outburst floods. *Sci. Total Environ.* **514**, 83–91 (2015).
- St. Pierre, K. A. et al. Drivers of mercury cycling in the rapidly changing glacierized watershed of the high Arctic's largest lake by volume (Lake Hazen, Nunavut, Canada). *Environ. Sci. Technol.* **53**, 1175–1185 (2019).
- Zdanowicz, C. et al. Accumulation, storage and release of atmospheric mercury in a glaciated Arctic catchment, Baffin Island, Canada. *Geochim. Cosmochim. Acta* **107**, 316–335 (2013).
- Paudyal, R. et al. Insights into mercury deposition and spatiotemporal variation in the glacier and melt water from the central Tibetan Plateau. *Sci. Total Environ.* **599–600**, 2046–2053 (2017).
- Sun, X. et al. The role of melting alpine glaciers in mercury export and transport: an intensive sampling campaign in the Quagaie Basin, inland Tibetan Plateau. *Environ. Pollut.* **220**, 936–945 (2017).

20. Vermilyea, A. W. et al. Continuous proxy measurements reveal large mercury fluxes from glacial and forested watersheds in Alaska. *Sci. Total Environ.* **599–600**, 145–155 (2017).
21. Nagorski, S. A. et al. Spatial distribution of mercury in southeastern Alaskan streams influenced by glaciers, wetlands, and salmon. *Environ. Pollut.* **184**, 62–72 (2014).
22. Lamarche-Gagnon, G. et al. Greenland melt drives continuous export of methane from the ice-sheet bed. *Nature* **565**, 73–77 (2019).
23. Linhoff, B. S. et al. Utility of  $^{222}\text{Rn}$  as a passive tracer of subglacial distributed system drainage. *Earth. Planet. Sci. Lett.* **462**, 180–188 (2017).
24. Zhang, L. & Wong, M. H. Environmental mercury contamination in China: sources and impacts. *Environ. Int.* **33**, 108–121 (2007).
25. Ram, A., Rokade, M. A., Borole, D. V. & Zingde, M. D. Mercury in sediments of Ulhas estuary. *Mar. Pollut. Bull.* **46**, 846–857 (2003).
26. Buck, C. S., Hammerschmidt, C. R., Bowman, K. L., Gill, G. A. & Landing, W. M. Flux of total mercury and methylmercury to the northern gulf of Mexico from U.S. Estuaries. *Environ. Sci. Technol.* **49**, 13992–13999 (2015).
27. Bowman, K. L., Lamborg, C. H. & Agather, A. M. A global perspective on mercury cycling in the ocean. *Sci. Total Environ.* **710**, 136166 (2020).
28. Diesler, M. et al. Molecular and biogeochemical evidence for methane cycling beneath the western margin of the Greenland Ice Sheet. *ISME* **8**, 2305–2316 (2014).
29. Christiansen, J. R. & Jørgensen, C. J. First observation of direct methane emission to the atmosphere from the subglacial domain of the Greenland Ice Sheet. *Sci. Rep.* **8**, 16623 (2018).
30. Morel, F. M. M., Kraepiel, A. M. L. & Amyot, M. The chemical cycle and bioaccumulation of mercury. *Annu. Rev. Ecol. Syst.* **29**, 543–566 (1998).
31. Weber, J. H. Review of possible paths for abiotic methylation of mercury(II) in the aquatic environment. *Chemosphere* **26**, 2063–2077 (1993).
32. Kellerman, A. M. et al. Glacier outflow dissolved organic matter as a window into seasonally changing carbon sources: Leverett Glacier, Greenland. *J. Geophys. Res. Biogeosci.* **125**, e2019JG005161 (2020).
33. Kohler, T. J. et al. Carbon dating reveals a seasonal progression in the source of particulate organic carbon exported from the Greenland Ice Sheet. *Geophys. Res. Lett.* **44**, 6209–6217 (2017).
34. Hawkings, J. R. et al. Enhanced trace element mobilization by Earth's ice sheets. *Proc. Natl Acad. Sci. USA* **117**, 31648–31659 (2020).
35. Møller, A. K. et al. Mercuric reductase genes (*merA*) and mercury resistance plasmids in high Arctic snow, freshwater and sea-ice brine. *FEMS Microbiol. Ecol.* **87**, 52–63 (2014).
36. Boyd, E. & Barkay, T. The mercury resistance operon: from an origin in a geothermal environment to an efficient detoxification machine. *Front. Microbiol.* **3**, <https://doi.org/10.3389/fmicb.2012.00349> (2012)
37. Bowman, K. L. et al. Distribution of mercury-cycling genes in the Arctic and equatorial Pacific oceans and their relationship to mercury speciation. *Limnol. Oceanogr.* **65**, S310–S320 (2020).
38. Parks, J. M. et al. The genetic basis for bacterial mercury methylation. *Science* **339**, 1332 (2013).
39. Herbert, L. C. et al. Glacial controls on redox-sensitive trace element cycling in Arctic fjord sediments (Spitsbergen, Svalbard). *Geochim. Cosmochim. Acta* **271**, 33–60 (2020).
40. Wang, K. et al. Subsurface seawater methylmercury maximum explains biotic mercury concentrations in the Canadian Arctic. *Sci. Rep.* **8**, 14465 (2018).
41. Cossa, D. et al. Sources, cycling and transfer of mercury in the Labrador Sea (Geotraces-Geovide cruise). *Mar. Chem.* **198**, 64–69 (2018).
42. Boutron, C. F., Vandal, G. M., Fitzgerald, W. F. & Ferrari, C. P. A forty year record of mercury in central Greenland snow. *Geophys. Res. Lett.* **25**, 3315–3318 (1998).
43. Nasr, M. & Arp, P. A. Mercury and organic matter concentrations in lake and stream sediments in relation to one another and to atmospheric mercury deposition and climate variations across Canada. *J. Chem.* **2017**, 8949502 (2017).
44. Kettles, I. M. & Shilts, W. W. *Geochemical and Lithological Composition of Surficial Sediments, Southeastern Ontario* (Geological Survey of Canada, 1996).
45. Tranter, M. & Wadham, J. L. in *Treatise on Geochemistry* 2nd edn (eds Turekian, H. D. & Holland, K. K.) 157–173 (Elsevier, 2014).
46. Scholz, H. & Baumann, M. An 'open system pingo' near Kangerlussuaq (Søndre Stromfjord). *West Greenl. Geol. Greenl. Surv. Bull.* **176**, 104–108 (1997).
47. Martos, Y. M. et al. Geothermal heat flux reveals the Iceland hotspot track underneath Greenland. *Geophys. Res. Lett.* **45**, 8214–8222 (2018).
48. Rysgaard, S., Bendtsen, J., Mortensen, J. & Sejr, M. K. High geothermal heat flux in close proximity to the Northeast Greenland Ice Stream. *Sci. Rep.* **8**, 1344 (2018).
49. Hawkings, J. R. et al. The effect of warming climate on nutrient and solute export from the Greenland Ice Sheet. *Geochem. Perspect. Lett.* **1**, 94–104 (2015).
50. Mankoff, K. D. et al. Greenland liquid water discharge from 1958 through 2019. *Earth Syst. Sci. Data* **12**, 2811–2841 (2020).

**Publisher's note** Springer Nature remains neutral with regard to jurisdictional claims in published maps and institutional affiliations.



**Open Access** This article is licensed under a Creative Commons Attribution 4.0 International License, which permits use, sharing, adaptation, distribution and reproduction in any medium or format, as long as you give appropriate credit to the original author(s) and the source, provide a link to the Creative Commons license, and indicate if changes were made. The images or other third party material in this article are included in the article's Creative Commons license, unless indicated otherwise in a credit line to the material. If material is not included in the article's Creative Commons license and your intended use is not permitted by statutory regulation or exceeds the permitted use, you will need to obtain permission directly from the copyright holder. To view a copy of this license, visit <http://creativecommons.org/licenses/by/4.0/>.

© The Author(s) 2021, corrected publication 2021

## Methods

**Site description.** *Kangerlussuaq (LG, RG and IS).* Glacial meltwater samples were collected from three land-terminating glacial catchments on the southwestern margin of the GrIS during the 2012 (LG), 2015 (LG) and 2018 (LG, RG and IS) sampled concurrently) summer ablation seasons. The three glacial catchments are east and northeast of Kangerlussuaq and drain west into the Isortoq River and Watson River (Fig. 1, ED1 and ED6). The hydrology of this sector of the GrIS is relatively well documented<sup>49,51–55</sup>, especially that of LG. All samples were collected from a fast-flowing location at the edge of the meltwater rivers draining the three glacial catchments.

LG extends ~80 km into the ice sheet interior, has a hydrologically active catchment area of ~600–900 km<sup>2</sup><sup>52,50</sup> and drains through a single portal on the northern side of the glacier snout (Extended Data Fig. 6a). Detailed documentation of the sampling site for LG can be found elsewhere<sup>22,33,56</sup>. LG samples were taken at 67.062° N, 50.201° W (2012, 2015) and 67.066° N, 50.215° W (2018). The 2018 sampling site was located approximately 1 km downstream of the 2012/2015 sampling site for logistical reasons.

RG is located to the north of LG (Fig. 1) and drains into Akuliarusiarsuup Kuua (Extended Data Fig. 6c). It was sampled in 2018 at 67.104° N, 50.217° W at the same location where hydrochemical gauging took place. The RG catchment is relatively poorly defined and comprises several sub-catchments with multiple outlets. More recent modelling estimates put the active catchment area at ~85 km<sup>2</sup> (including the 'Point 660' sub-catchment defined in ref.<sup>53</sup>) and the distance it extends inland at ~10–15 km (refs.<sup>20,57</sup>).

IS is located to the north of both the LG and RG catchments. The glacier drains into Isortoq River to the west (Extended Data Fig. 6b), where samples were taken and hydrological gauging performed at 67.166° N, 50.889° W in 2018. It extends over 120 km into the GrIS from the ice margin and covers approximately 3,200 km<sup>2</sup> (to an altitude of 1,750 m; Fig. 1)<sup>53</sup> and approximately 7,300 km<sup>2</sup> to the ice divide<sup>50</sup>.

*NK/AF.* NK (Godthåbsfjord) is one of the best-studied fjords in Greenland (Fig. 1)<sup>14,58–60</sup>. It is ~190 km long, up to 8 km wide, has a mean depth of 260 m and covers an area >2,000 km<sup>2</sup>. Glacial meltwater enters the fjord through a combination of land- and marine-terminating glaciers, of which three are major marine-terminating glaciers (Narsap Sermia, Akullersuup Sermia and Kangiata Nunaata Sermia) and three are land-terminating glacial inputs (Kangilinnuata Sermia, Qamaarsuup Sermia and Saqqap Sermersua). Freshwater inputs during the summer ablation season drive an estuarine circulation with a low-salinity surface plume flowing toward the fjord mouth to the west<sup>61</sup>. Meltwater input into the fjord is estimated to be ~20 km<sup>3</sup> year<sup>-1</sup>, with roughly a 50% contribution from marine- and 50% from land-terminating glaciers, and minor inputs from non-glacial tundra runoff<sup>60</sup>. All glaciers have experienced thinning and accelerating retreat over the past two decades, echoing other outlet glaciers of the GrIS<sup>60</sup>.

AF is located to the south of NK (Fig. 1). Glacial meltwater enters the fjord from a single land-terminating glacier, Kangaarsuup Sermia. The freshwater input from the river at the head of AF is estimated to be 2.4 km<sup>3</sup> year<sup>-1</sup> (1.8–3.7 km<sup>3</sup> year<sup>-1</sup>), with meltwater runoff contributing >75 % of total discharge (mean of Modèle Atmosphérique Régional (MAR)-generated liquid water runoff from 2008 to 2017 (ref.<sup>59</sup>)).

**Hydrological monitoring.** Hydrological monitoring of LG has been described in detail multiple times elsewhere<sup>49,51,52</sup>, and the same approach was taken for all catchments in this study. In brief, LG was hydrologically gauged at a stable bedrock section throughout the 2012 and 2015 ablation seasons (late April to end of August) and LG, IS and RG during a 3-week period in 2018. A package of hydrochemical sensors connected to a datalogger (Campbell Scientific CR1000 or CR800) were deployed to record pH (Honeywell Durafet), water temperature (Campbell Scientific), electrical conductivity (Campbell Scientific 547 or Keller-Druck DCX-22-CTD, calibrated with an 84 µS cm<sup>-1</sup> conductivity standard before deployment), turbidity (Partech C or Turner Designs Cyclops-7<sup>T</sup> turbidity sensor) and stage (HOBO pressure transducer) at each sampling site. Stage was converted to discharge using a rating curve determined from rhodamine dye-dilution experiments ( $n = 41$  during 2012,  $n = 25$  during 2015 at LG; and  $n = 8, 6$  and  $9$  at LG, IS and RG, respectively, during 2018). Uncertainties on discharge measurements were calculated using the root-mean-square error and are estimated as  $\pm 10.7$ – $12.1$ %. Turbidity was converted to suspended sediment concentration (SSC) using a calibration of manual sediment samples collected against the turbidity recorded at the time of sampling<sup>52</sup>. Uncertainties in SSC are estimated to be  $\pm 6$ % (ref.<sup>53</sup>).

### Sample collection, processing and storage. Trace metal clean sampling.

All samples were collected according to strict trace metal clean protocols. Sampling bottles (15/250-mL low-density polyethylene (LDPE) bottles and 250/500/1,000-mL fluorinated high-density polyethylene (FI-HDPE) bottles) and syringes were cleaned sequentially in 1% DECON (~24 h), trace metal grade 3 M HCl (~48 h), followed by trade metal grade 3 M HNO<sub>3</sub> (~48 h) and thoroughly rinsed with ultra-pure water (UPW; Milli-Q, 18.2 MΩ cm<sup>-1</sup>) in between cleaning stages before drying under a laminar flow hood (ISO 5). Whatman GD/XP

polyethersulphone (PES) 0.45 µm and Whatman Anotop 25 0.02 µm syringe filters were cleaned with ultra-trace metal grade HCl (Optima<sup>®</sup>). The 0.45 µm syringe filters were cleaned by passing through 20 mL of 1.2 M HCl, with the final ~1 mL acidic cleaning solution allowed to sit in the filter for ~2 h before rinsing with 40 mL of UPW and flushing with laminar flow filtered air to dry. The 0.02 µm filters were cleaned by passing 20 mL of 0.02 M HCl, followed immediately by 20 mL of UPW and clean laminar flow filtered air to dry. A portable peristaltic pump or Teflon diaphragm pump and filter capsules were used for sample collection in 2018 (see 'LG/RG/IS 2018' and 'NK/AF 2018'). Peristaltic pump tubing was soaked in 1.2 M trace-metal grade HCl for 24 h and rinsed by pumping several litres of ultra-pure water through it before use. AcroPak 500 capsule filters (0.45 µm with Supor PES membrane) were thoroughly flushed with sample water (several hundred millilitres) before collection of the final sample.

*LG/SS 2012.* Total particulate Hg was determined on ten samples taken at LG intermittently from 16 May to 11 July 2012. Meltwater was collected in a borosilicate glass bottle, taken to a laboratory tent and immediately filtered through a 0.22 µm membrane filter (PES) with the sediment retained on the filter. Filters were stored air-dried and cool before analysis. Three samples for total dissolved Hg (dHg) were also taken downstream of LG from a salinity gradient in surface waters of SS (ca. 25 km downstream of LG) on 16 June, using the same protocols as particulate Hg samples above, with the 0.22 µm filtrate stored in 250-mL acid-washed borosilicate glass bottles and stored cool in the dark before analysis (Extended Data Fig. 5).

*LG 2015.* Samples were collected from 1 May to 28 July 2015. Samples from 80 time points were size fractionated (0.02 + 0.45 µm) for total filterable Hg concentrations, and an additional sample was taken from a geothermal spring located 400 m in front of the glacier terminus on 28 July<sup>46</sup>. Bulk water samples were collected in 250-mL or 1000-mL LDPE bottles, zip-lock bagged and taken immediately to a designated 'clean' laboratory tent (no shoes, hairnets and strict cleaning protocols observed) for processing. Bulk samples were filtered through a 0.45 µm syringe filter (12 mL to waste and rinse, with final 10 mL collected), then through a stack of 0.45 µm/0.02 µm syringe filters (12 mL to waste and rinse with final 10 mL collected; see 'Trace metal clean sampling'). These filtered samples were immediately preserved with Optima grade HNO<sub>3</sub> to a final acidity of 0.074 M according to Environmental Protection Agency (EPA) method 245.1 and stored individually double zip-lock bagged in the dark and refrigerated as soon as possible (maximum of 2 weeks).

Although Hg storage in LDPE bottles is not advisable for low-level Hg analysis<sup>52,63</sup>, short-term storage of samples (~weeks) for total Hg analysis with elevated concentrations when acidified is likely to be acceptable<sup>64</sup>. Loss or enrichment of Hg due to transmission through plastic of volatile Hg<sup>0</sup> is the most likely storage artefact<sup>63</sup> due to the porosity of unfluorinated polyethylene. A study has shown a >10 ng L<sup>-1</sup> (~50 pM) enrichment in samples stored in LDPE over a period of 5 weeks (refs.<sup>65</sup>). This corresponds to ~15% of the discharge-weighted mean concentration of sHg and 3.2% of the discharge-weighted mean concentration of cHg from LG in 2015, assuming a worst-case scenario of 200 pM contamination over the storage to measurement period of ~120 days. Furthermore, any contamination effect should be reflected in the procedural blanks.

*LG/RG/IS 2018.* Samples were collected concurrently at three glaciers over a 25-day period in 2018 from 19 June to 14 July to determine dissolved inorganic Hg (dIHg, as Hg<sup>2+</sup>) and dissolved methylmercury (dMeHg) concentrations. Sample collection took place at 11:00 at LG and RG, and 15:00 at IS on the same days, the latter delayed by 4 h to account for the water transit time from the glacier terminus to the sampling site ~26 km downstream (that is, to capture a body of water similar to the two other sampling locations; Fig. 1). Bulk water samples were collected in acid-cleaned 1000-mL FI-HDPE bottles and taken immediately for processing in a laboratory tent or field laboratory. Water was filtered through a 0.45 µm AcroPak 500 capsule filter using a peristaltic pump and acid-cleaned C-Flex tubing into 250-mL FI-HDPE bottles after rinsing with three aliquots of filtered water. Samples were immediately acidified using ultra trace metal grade (Optima) HCl to a final concentration of 0.048 M (0.4% v/v concentrated HCl). Sample bottles were double zip-lock bagged and stored in the dark until returning to the University of Bristol, where they were transferred to refrigerated storage.

*NK/AF 2018.* Samples were collected from the surface waters of two fjord systems during a cruise in July 2018 (5 July–9 July). Trace metal clean sampling was undertaken using a towfish system coupled to acid-cleaned polyvinylchloride tubing, a Teflon diaphragm pump (A2CH1 F8 AstiPure II, Saint Gobain) and final filtration through a 0.45 µm AcroPak 500 capsule filter. The towfish comprised a plastic fin held ~1.5 m underwater by ~25 kg of epoxy-covered dive weights. Samples were filtered into 500-mL FI-HDPE bottles after rinsing three times with filtered sample water, then acidified using ultra trace metal grade (Optima) HCl to a final concentration of 0.048 M (0.4% v/v concentrated HCl) and stored refrigerated until analysis.



**Geochemical analysis. Particulate and total dissolved mercury (2012).** Particulate and total dissolved mercury concentrations were determined at the Woods Hole Oceanographic Institution. Filters were first oven dried at 55 °C overnight before being digested in ultra trace metal grade 2 M HNO<sub>3</sub> (refs. 65,66.) Briefly, filters were placed in pre-cleaned 15-mL polypropylene centrifuge tubes, and 8 mL of acid was added. Tubes were inverted to mix then placed in an ultrasonic bath at 55 °C for 15 min. Samples were then centrifuged for 5 min at 3,000 rpm, and supernatant retained in a new, clean tube for total Hg analysis.

Total Hg in leach solutions and in filtered fjord samples was determined by cold vapour atomic fluorescence spectroscopy (CV-AFS) following EPA method 1631. Samples were digested with bromine monochloride (BrCl) and then reduced with stannous chloride (SnCl<sub>2</sub>) and quantified by dual Au-amalgamation CV-AFS using an external standard calibration curve. Filter blanks processed as per samples were all below the instrumental limit of detection (<0.5 pM).

**Total dissolved mercury (2015).** Total dissolved Hg in 0.02 and 0.45 µm filtered samples were determined using a Thermo Scientific XSERIES 2 quadrupole ICP-MS with collision/reaction cell after acidification of samples to 1% (v/v) HCl (laboratory distilled ultra trace metal grade) at the National Oceanography Centre in Southampton, within 3 months of sample collection. This method is sub-optimal for analysis of Hg due to a memory effect and very high first ionization potential in ICP-MS analysis, leading to low sensitivity and prolonged sample washout. Several measures of analytical quality were noted to ensure reliable results. For example, the analytical precision over the concentration range observed in samples was ±23.4%. Sample memory effects (a common issue in Hg ICP-MS analysis), determined by running a high-concentration sample followed by five analytical blanks, was high at ~400 pM in the first blank to <100 pM in the final blank. Procedural blanks (*n* = 16) taken in the field using transported ultra-pure water and the same procedure as samples, run intermittently throughout the run, averaged 522 ± 255 pM, and the mean was subtracted from measured values before reporting. It is expected that a large fraction, if not all, of this (~400 pM), is due to the system memory effect or storage contamination in LDPE bottles, further highlighting that this methodology is not suitable for low-level Hg analysis. The detection limit (mean of ten blanks + standard deviation × 3) was therefore high at 800 pM, and all blanks fell under this. A subset of samples were also analysed by CV-AFS (as per section 4.1) in a separate Hg laboratory (Greg Carling at BYU) with blank values <200 pM and similarly high sample concentrations that correlated to those reported via ICP-MS (*R*<sup>2</sup> = 0.58) with a positive offset for CV-AFS samples (~1,000 pM), despite 4 years of storage time, which would otherwise be deemed unacceptable. The higher values reported for the CV-AFS method are likely either due to underreporting by ICP-MS, or sample contamination over the prolonged storage period<sup>63</sup>. The discharge-weighted mean concentrations for sHg in 2015 (1,400 pM) are similar to discharge-weighted mean dIHg concentrations in 2018 (603–1,260 pM; Supplementary Table 1), the latter of which were collected and measured in a Hg-clean manner. This gives additional confidence that the 2015 reported values are reliable within the estimated uncertainty (~±30%).

**Dissolved inorganic Hg<sup>0</sup>/Hg<sup>2+</sup> and dissolved MeHg (2018).** Dissolved inorganic Hg<sup>2+</sup> and dissolved MeHg in glacial meltwater samples were determined in the High Magnetic Field Laboratory Mercury Lab. Both Hg species were detected simultaneously after direct aqueous ethylation<sup>67</sup>, purge and trap, separation via gas chromatography and detection using CV-AFS, on a Tekran 2700 system using EPA method 1630 with adaptations from Mansfield and Black<sup>68</sup>. Briefly, samples were diluted 1:15 with Hg-free ultra-pure water (Milli-Q, 18.2 MΩ cm<sup>-1</sup>), buffered to pH 4.1 and ethylated with NaBEt<sub>3</sub> to a final concentration of 40 µM. Glacial meltwater samples had very low DOC concentrations (<20 µM) and were found suitable for the direct ethylation technique without distillation or addition of NaCl (ref. 68). Spiked samples (*n* = 12, spike values: Hg<sup>2+</sup> concentration of 10 pM, MeHg concentration of 2 pM) displayed mean Hg<sup>2+</sup> recovery values of 98% (95–100%) and MeHg spike recoveries of 103% (77–111%). Precision values based on replicate analysis (*n* = 5) of 10 pM Hg<sup>2+</sup> standards and 2 pM MeHg standards placed randomly throughout the analytical run were ±3.1% and ±9.1% respectively. Blanks were below instrumental detection limits for both Hg<sup>2+</sup> (~<1 pM) and MeHg (~<0.1 pM).

Fjord samples were analysed using techniques similar to those above. MeHg and Hg<sup>2+</sup> concentrations were determined following Mansfield and Black<sup>68</sup> with addition of NaCl before direct aqueous ethylation using NaBEt<sub>3</sub>. Samples were diluted 1:2 in Hg-free UPW (Milli-Q, 18.2 MΩ cm<sup>-1</sup>) and buffered to pH 4.1 (using 3 M sodium acetate/acetic acid buffer), followed by NaCl addition to a final concentration of 1.2 M and direct ethylation with addition of NaBEt<sub>3</sub> to a final concentration of 40 µM. Spiked samples (*n* = 12, spike values: Hg<sup>2+</sup> concentration of 10 pM, MeHg concentration of 1 pM) displayed mean Hg<sup>2+</sup> recovery values of 117% (78–153%) and MeHg recoveries of 104% (88–119%). MeHg precision was ±8.3%, calculated from five replicate standards (1 pM) run randomly throughout the analytical run, while Hg<sup>2+</sup> precision using the direct ethylation technique was ±11.7%. Three NaCl blanks (that is, blanks treated exactly the same as samples with 1.2 M NaCl addition) were below the detection limit for MeHg

(<0.1 pM), and were ~1 pM for Hg<sup>2+</sup>. Total dissolved Hg was also determined independently in two other Hg laboratories using CV-AFS and EPA method 1631 (Greg Carling and Carl Lamborg) as in 'Particulate and total dissolved mercury (2012)'. Differences between the total dissolved Hg concentration in the three laboratories were ±23% (±8–42%). Mean total dissolved concentration from all three measurements are used as the reported value for TdHg (Fig. 4) along with individual error based on the standard deviation of the three concentrations reported by individual laboratories.

**Dissolved organic carbon (2018).** Samples for DOC concentrations were filtered using 0.45 µm Whatman Aqua 30 syringe filters into acid-washed HDPE bottles (10% HCl v/v for 48 h) and kept frozen in the dark until analysis. DOC concentrations were measured after acidification using a Shimadzu TOC-L<sub>CHN</sub> analyser with high-sensitivity catalyst. Sample concentrations were calculated from a manual calibration curve based on standards (0.05–2 mg CL<sup>-1</sup>), gravimetrically prepared from a certified TOC standard of potassium hydrogen naphthalate (1,000 ± 10 mg CL<sup>-1</sup>; Sigma Aldrich). The limit of quantification (LOQ) was 0.026 mg L<sup>-1</sup> (where LOQ = LOB + 5 × s.d. of low-concentration sample, where LOB is the limit of baseline)<sup>69</sup>. Precision was calculated from repeat standard measurements of 0.10 and 0.50 mg CL<sup>-1</sup> and was better than ±5%.

**Microbiological analysis (2015).** Samples for microbiological analysis were taken at the portal of LG during May–July 2015 concurrently with samples taken for geochemical analysis to identify genes associated with Hg cycling in the subglacial microbial community. Water samples were passed through a Sterivex syringe filter (0.22 µm; Millipore) using a sterile syringe until clogged (~300 mL). Water was flushed from the filter chamber, filled with nucleic acid preservation buffer (LifeGuard, QIAGEN) and immediately frozen in the field at -20 °C. Total DNA in suspended sediment retained in the Sterivex filter was extracted using the PowerWater Sterivex DNA isolation kit (MO BIO). A full description of microbiological sample collection and DNA extraction can be found in refs. 22,70, as the extracts sequenced for metagenomes here consisted of subsamples of those used for 16S rRNA gene analysis in the cited studies.

Four pooled samples were used for metagenomic sequencing due to the low DNA content of individual extracts and cost. Pool 1 represented early-season assemblages (three daily samples in the period from 4 May to 7 June), pool 2 represented 'early' outburst events (five daily samples in the period from 20 June to 2 July), pool 3 represented 'late' outburst events (four daily samples in the period from 5 to 10 July) and pool 4 represented late season (four daily samples in the period from 13 July onward) when an efficient drainage system was established. A total of at least 20 ng of treated DNA from each pooled sample served as the input for the TruSeq Nano DNA library preparation kit (Illumina). Insert length ranged between 295 and 409 bp. DNA libraries were prepared using a TruSeq Nano DNA LT kit and sequenced (2 × 150 bp) in four lanes of Illumina NextSeq500 using a High-Output V2-300 kit at the Bristol Genomics Facility. The four metagenomes obtained were assembled as follows: reads were trimmed by removing adapters with Trimmomatic using Illumina TruSeq2-PE adapters with a seed mismatch threshold, palindrome clip threshold and simple clip threshold set at 2, 30 and 10, respectively. Sequencing reads were quality filtered by base call quality using the FASTX-Toolkit, specifically fastq\_quality\_filter, with the following parameters: -Q33 -q 30 -p 50. The paired-end assembly of the remaining reads was performed with the MEGAHIT assembler (v. 1.1.3) with the following parameters: megahit -1 all.pe.qc.fq.1 -2 all.pe.qc.fq.2 -r all.se.qc.fq -o all.megahit.assembly. Reads from all samples were assembled together. A total of 9,168,354 contigs were obtained, with an average length of 618.7 bp; N50 was 712 bp. The total length of the assembled metagenome reached 5,672,583,505 bp, while the longest contig had 297,443 bp. Assembled data were annotated using the MG-RAST automated pipeline against the RefSeq database. For phylogenetic analyses, homologues of translated *merA* sequences were found using BLASTP against the National Center for Biotechnology Information nr database<sup>71</sup>. Representatives of known main lineages were also added. Sequences were aligned in MAFFT v. 7<sup>72</sup> and trimmed manually. The phylogenetic tree (Extended Data Fig. 4) was determined by Phylml v. 3.1<sup>73</sup> under the LGgamma model and non-parametric bootstrap analysis with 100 replicates.

**Statistical analyses.** All statistical analyses were performed in JMP Pro 15 (SAS). Student's *t* test was used to determine whether population means were statistically different. Linear correlations were used to determine the strength of relationship between two variables and the significance of the correlation. *P* values are presented in the main text with *P* < 0.05 assumed to be statistically significant.

**Flux estimations. Discharge-weighted mean method.** The first-order flux estimates presented in Table 1 are calculated using the discharge-weighted mean concentrations from the three 2018 sampling sites, where the most complete IHg and MeHg record is present. The discharge-weighted concentration was then multiplied by the mean annual modelled meltwater discharge from the southwestern margin of the GrIS (2009–2018; Extended Data Fig. 2) from ref. 50 to generate dIHg and dMeHg flux estimates for southwest Greenland.

**LOADEST method.** Catchment fluxes were also estimated using the constituent-load modelling software LOADEST<sup>74</sup>, with measured 2018 mercury concentrations and mean daily discharge. Regression models for concentrations were generated using the adjusted maximum-likelihood estimator and automatic best model selection (model 0) to allow for model selection based on the Akaike information criterion. Total annual fluxes were estimated using the mean concentration output of the model with the modelled meltwater discharge detailed in Table 1, with uncertainty defined as the modelled concentrations at the 25th and 75th percentiles. These data are presented in Supplementary Table 2. Mean flux estimates deviated  $\pm 0.7$ – $7.6\%$  from those calculated using the discharge-weighted mean concentrations in Table 1.

**Representativeness of the study area.** There are obvious limitations to using three glaciers to estimate Hg export from the southwestern margin of the GrIS. We acknowledge that IS, LG and RG collectively cover a small proportion of the ice sheet ( $\sim 0.3\%$  by surface area) and southwestern Greenland ( $\sim 4.1\%$ ). However, the area is significantly larger (by almost two orders of magnitude) than any other glacier study area investigated thus far in the literature (both in Greenland and worldwide), and to our knowledge, this is the only study to date that has measured Hg concentrations in ice sheet runoff (rather than disconnected ice caps in Greenland). Furthermore, the annual discharge of these three outlets equates to nearly 8% of the runoff from the southwestern sector of the GrIS. The Kangerlussuaq area is an excellent analogue study area for the southwestern region of the GrIS for several other reasons that have been documented in previous studies, including the underlying geology, hydrology and because its discharge is proportional to total modelled ice sheet runoff<sup>49,51,75–78</sup>. The underlying debris and morphology of the catchment are similar to other catchments of southwestern GrIS<sup>79</sup> (Extended Data Fig. 2), and bedrock geology is predominantly Neoproterozoic gneiss/granite, which is typical of large areas of the crystalline rocks that dominate the Precambrian Shield on which Greenland lies<sup>75,80</sup> (Extended Data Fig. 1). The catchment hydrology here is also believed typical of the large Greenland outlet glaciers that dominate discharge of meltwaters from the GrIS<sup>76–78,81</sup>.

## Data availability

All data contained in this article that are not included in tables are freely available (<https://doi.org/10.5281/zenodo.4634280>). The metagenomic data are accessible in MG-RAST under the number 4765056.3.

## References

- Bartholomew, I. et al. Supraglacial forcing of subglacial drainage in the ablation zone of the Greenland Ice Sheet. *Geophys. Res. Lett.* **38**, L08502 (2011).
- Cowton, T., Nienow, P., Bartholomew, I., Sole, A. & Mair, D. Rapid erosion beneath the Greenland Ice Sheet. *Geology* **40**, 343–346 (2012).
- Lindbäck, K. et al. Subglacial water drainage, storage, and piracy beneath the Greenland Ice Sheet. *Geophys. Res. Lett.* **42**, 7606–7614 (2015).
- Rennermalm, A. K. et al. Proglacial river stage, discharge, and temperature datasets from the Akuliarisarsuup Kuua River northern tributary, Southwest Greenland, 2008–2011. *Earth Syst. Sci. Data* **4**, 1–12 (2012).
- Nienow, P. W., Sole, A. J., Slater, D. A. & Cowton, T. R. Recent advances in our understanding of the role of meltwater in the Greenland Ice Sheet system. *Curr. Clim. Change Rep.* **3**, 330–344 (2017).
- Hawkings, J. R. et al. The silicon cycle impacted by past ice sheets. *Nat. Commun.* **9**, 3210 (2018).
- van de Wal, R. S. W. & Russell, A. J. A comparison of energy balance calculations, measured ablation and meltwater runoff near Søndre Stromfjord, West Greenland. *Glob. Planet. Chang.* **9**, 29–38 (1994).
- Hopwood, M. J. et al. Seasonal changes in Fe along a glaciated Greenlandic fjord. *Front. Earth Sci.* **4**, <https://doi.org/10.3389/feart.2016.00015> (2016).
- Meire, L. et al. High export of dissolved silica from the Greenland Ice Sheet. *Geophys. Res. Lett.* **43**, 9173–9182 (2016).
- Van As, D. et al. Increasing meltwater discharge from the Nuuk region of the Greenland Ice Sheet and implications for mass balance (1960–2012). *J. Glaciol.* **60**, 314–322 (2014).
- Mortensen, J. et al. On the seasonal freshwater stratification in the proximity of fast-flowing tidewater outlet glaciers in a sub-Arctic sill fjord. *J. Geophys. Res. Oceans* **118**, 1382–1395 (2013).
- Hammerschmidt, C. R., Bowman, K. L., Tabatchnick, M. D. & Lamborg, C. H. Storage bottle material and cleaning for determination of total mercury in seawater. *Limnol. Oceanogr. Methods* **9**, 426–431 (2011).
- Parker, J. L. & Bloom, N. S. Preservation and storage techniques for low-level aqueous mercury speciation. *Sci. Total Environ.* **337**, 253–263 (2005).
- Hall, G. E. M., Pelchat, J. C., Pelchat, P. & Vaive, J. E. Sample collection, filtration and preservation protocols for the determination of 'total dissolved mercury in waters. *Analyst* **127**, 674–680 (2002).
- Hammerschmidt, C. R. & Fitzgerald, W. F. Formation of artifact methylmercury during extraction from a sediment reference material. *Anal. Chem.* **73**, 5930–5936 (2001).
- Balcom, P. H., Hammerschmidt, C. R., Fitzgerald, W. F., Lamborg, C. H. & O'Connor, J. S. Seasonal distributions and cycling of mercury and methylmercury in the waters of New York/New Jersey Harbor Estuary. *Mar. Chem.* **109**, 1–17 (2008).
- Liang, L., Horvat, M. & Bloom, N. S. An improved speciation method for mercury by GC/CVAFS after aqueous phase ethylation and room temperature precollection. *Talanta* **41**, 371–379 (1994).
- Mansfield, C. R. & Black, F. J. Quantification of monomethylmercury in natural waters by direct ethylation: interference characterization and method optimization. *Limnol. Oceanogr. Methods* **13**, e10009 (2015).
- Armbruster, D. A. & Pry, T. Limit of blank, limit of detection and limit of quantitation. *Clin. Biochem. Rev.* **29**(Suppl 1), S49–S52 (2008).
- Lamarche-Gagnon, G. et al. Meltwater runoff from the Greenland Ice Sheet reveals microbial consortia from contrasting subglacial drainage systems. Preprint at *bioRxiv* <https://doi.org/10.1101/2020.05.26.116566> (2020).
- Altschul, S. F. et al. Gapped BLAST and PSI-BLAST: a new generation of protein database search programs. *Nucleic Acids Res.* **25**, 3389–3402 (1997).
- Katoh, K., Rozewicki, J. & Yamada, K. D. MAFFT online service: multiple sequence alignment, interactive sequence choice and visualization. *Brief. Bioinform.* **20**, 1160–1166 (2019).
- Guindon, S. et al. New algorithms and methods to estimate maximum-likelihood phylogenies: assessing the performance of PhyML 3.0. *Syst. Biol.* **59**, 307–321 (2010).
- Runkel, R. L., Crawford, C. G. & Cohn, T. A. in *Techniques and Methods Book 4* (US Geological Survey, 2004).
- Henriksen, N., Higgins, A. K., Kalsbeek, F. & Pulvertaft, T. C. R. Greenland from Archaean to Quaternary descriptive text to the 1995 geological map of Greenland, 1:2,500,000. 2nd edition. *GEUS Bull.* **18**, 1–126 (2009).
- Tedstone, A. J. et al. Greenland ice sheet motion insensitive to exceptional meltwater forcing. *Proc. Natl Acad. Sci. USA* **110**, 19719–19724 (2013).
- Chandler, D. M. et al. Evolution of the subglacial drainage system beneath the Greenland Ice Sheet revealed by tracers. *Nat. Geosci.* **6**, 195–198 (2013).
- Chu, V. W. Greenland ice sheet hydrology: a review. *Prog. Phys. Geogr.* **38**, 19–54 (2014).
- Knight, P. G., Waller, R. I., Patterson, C. J., Jones, A. P. & Robinson, Z. P. Discharge of debris from ice at the margin of the Greenland Ice Sheet. *J. Glaciol.* **48**, 192–198 (2002).
- Kalsbeek, F. The evolution of the precambrian shield of Greenland. *Geol. Rundsch.* **71**, 38–60 (1982).
- Cowton, T. et al. Evolution of drainage system morphology at a land-terminating Greenlandic outlet glacier. *J. Geophys. Res. Earth* **118**, 29–41 (2013).
- Dawes, P. R. The bedrock geology under the inland ice: the next major challenge for Greenland mapping. *Geol. Surv. Den. Greenl.* **17**, 57–60 (2009).
- White, L. F. et al. Tracking the provenance of Greenland-sourced, Holocene aged, individual sand-sized ice-rafted debris using the Pb-isotope compositions of feldspars and <sup>40</sup>Ar/<sup>39</sup>Ar ages of hornblendes. *Earth. Planet. Sci. Lett.* **433**, 192–203 (2016).

## Acknowledgements

This research is part of a European Commission Horizon 2020 Marie Skłodowska-Curie Actions fellowship ICICLES (grant agreement #793962) to J.R.H. Greenland terrestrial research campaigns were funded by a UK NERC standard grant (NE/I008845/1) and a Leverhulme Trust Research Grant (RPG-2016-439) to J.L.W., with additional support provided by a Royal Society Wolfson Merit Award to J.L.W. Additional funding came from Czech Science Foundation grants (GACR: 15-17346Y and 18-12630S) to M.S. Fjord fieldwork was supported by European Research Council grant ICY-LAB (grant agreement 678371) and Royal Society Enhancement Award (grant RGF\EA\181036) to K.R.H. L.M. was funded by research programme VENI (0.16.Veni.192.150, NWO). T.J.K. was supported by Charles University Research Centre program no. 204069. The authors thank the captain and crew of the RV *Kisaq* and staff at the Greenland Institute of Natural Resources for assistance during fjord fieldwork, and all those involved with fieldwork at Leverett Camp during the 2012 and 2015 field campaigns. M. Cooper is thanked for providing the geological overview file for Extended Data Fig. 1a, and K. Mankoff for help in generating the modelled GrIS discharge datasets. The authors also thank G. White in the geochemistry group at the National High Magnetic Field Geochemistry Laboratory, which is supported by NSF DMR-1644779 and the State of Florida, for analytical support. The authors acknowledge past and present Greenlandic people as stewards of the land and sea where this research took place.

## Author contributions

J.R.H., B.S.L., J.L.W. and S.T. conceived the project. J.R.H., B.S.L., M.S., R.W., K.R.H., G.L.-G., T.J.K., A.M.K., K.A.C., J.E.H., A.D.H., P.V., S.H., M.B. and L.M. performed the

fieldwork, collected samples and provided essential logistical support. J.R.H., B.S.L., C.H.L., G.T.C., G.L.-G., T.J.K., L.F., T.V. and M.S. undertook the geochemical and microbiological analyses, and associated data processing. J.L.W., M.S., K.R.H., R.G.M.S. and J.R.H. funded the research. J.R.H. analysed the data and wrote the manuscript with significant input from B.S.L., J.L.W., M.S., C.H.L., G.T.C. and R.G.M.S., with contributions from all other co-authors.

### Competing interests

The authors declare no competing financial interests.

### Additional information

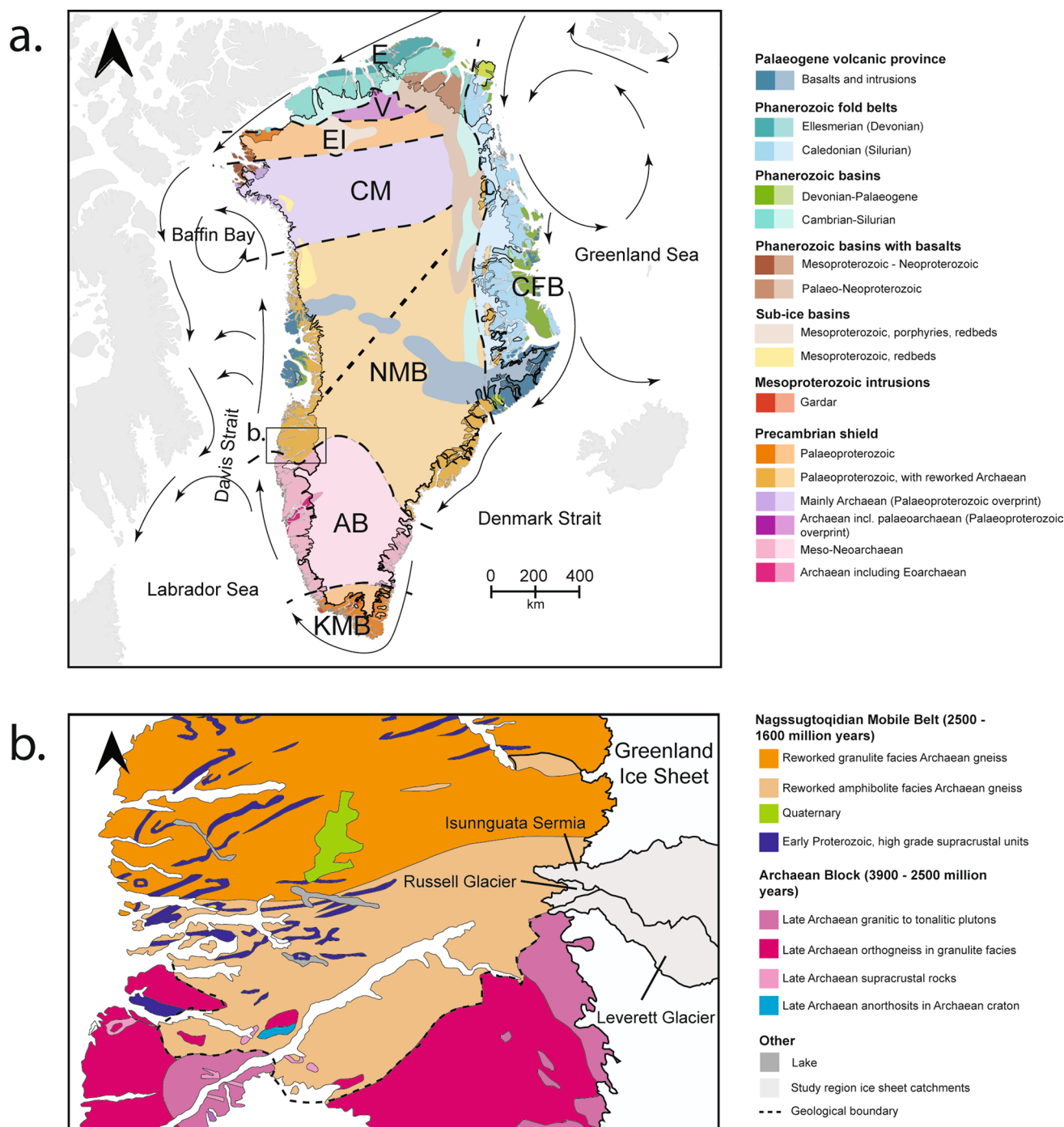
**Extended data** is available for this paper at <https://doi.org/10.1038/s41561-021-00753-w>.

**Supplementary information** The online version contains supplementary material available at <https://doi.org/10.1038/s41561-021-00753-w>.

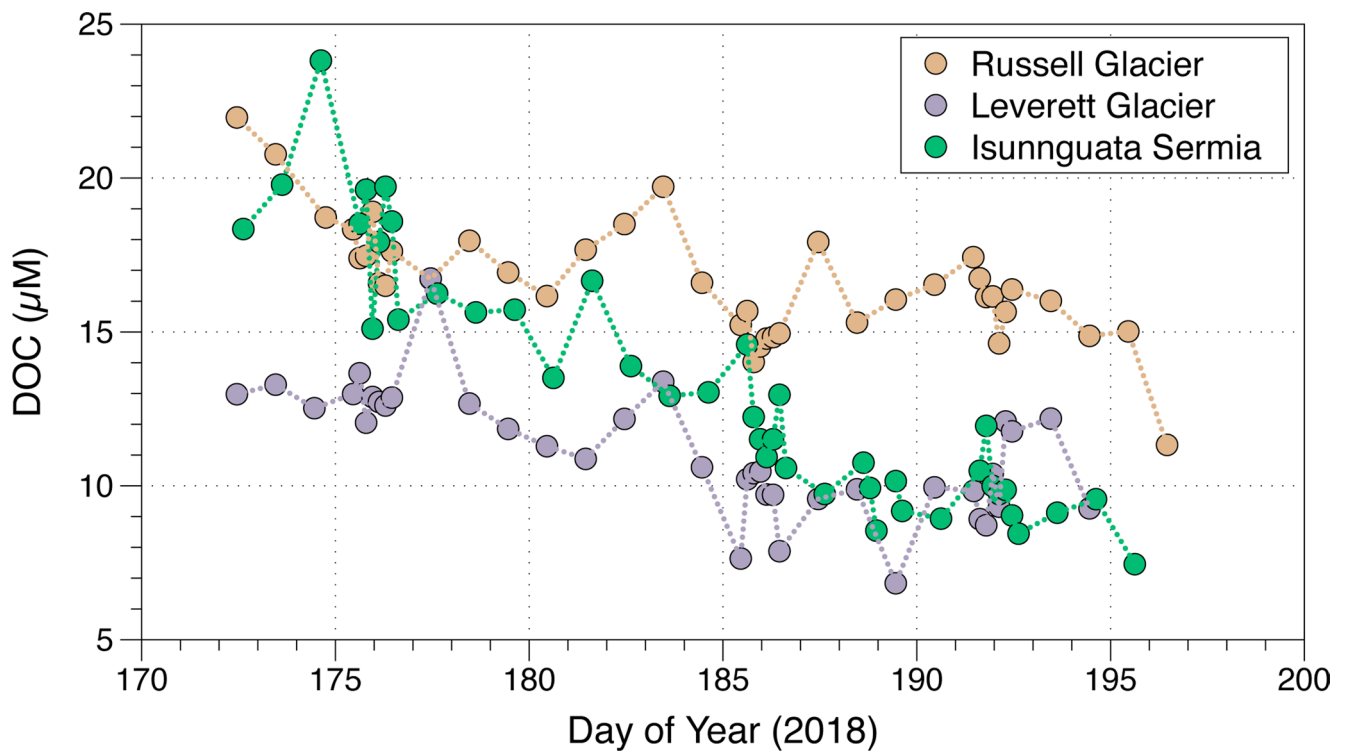
**Correspondence and requests for materials** should be addressed to J.R.H.

**Peer review information** *Nature Geoscience* thanks the anonymous reviewers for their contribution to the peer review of this work. Primary Handling Editor: Xujia Jiang.

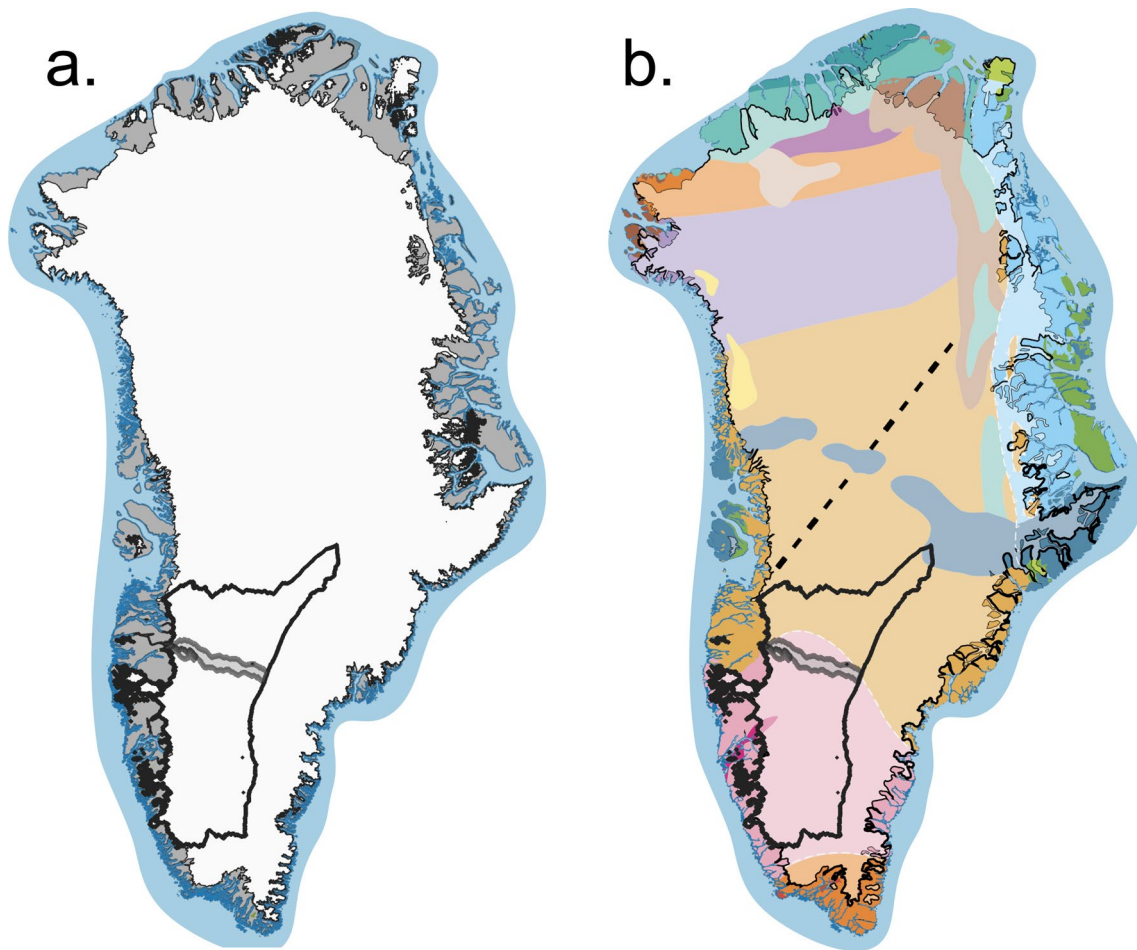
**Reprints and permissions information** is available at [www.nature.com/reprints](http://www.nature.com/reprints).



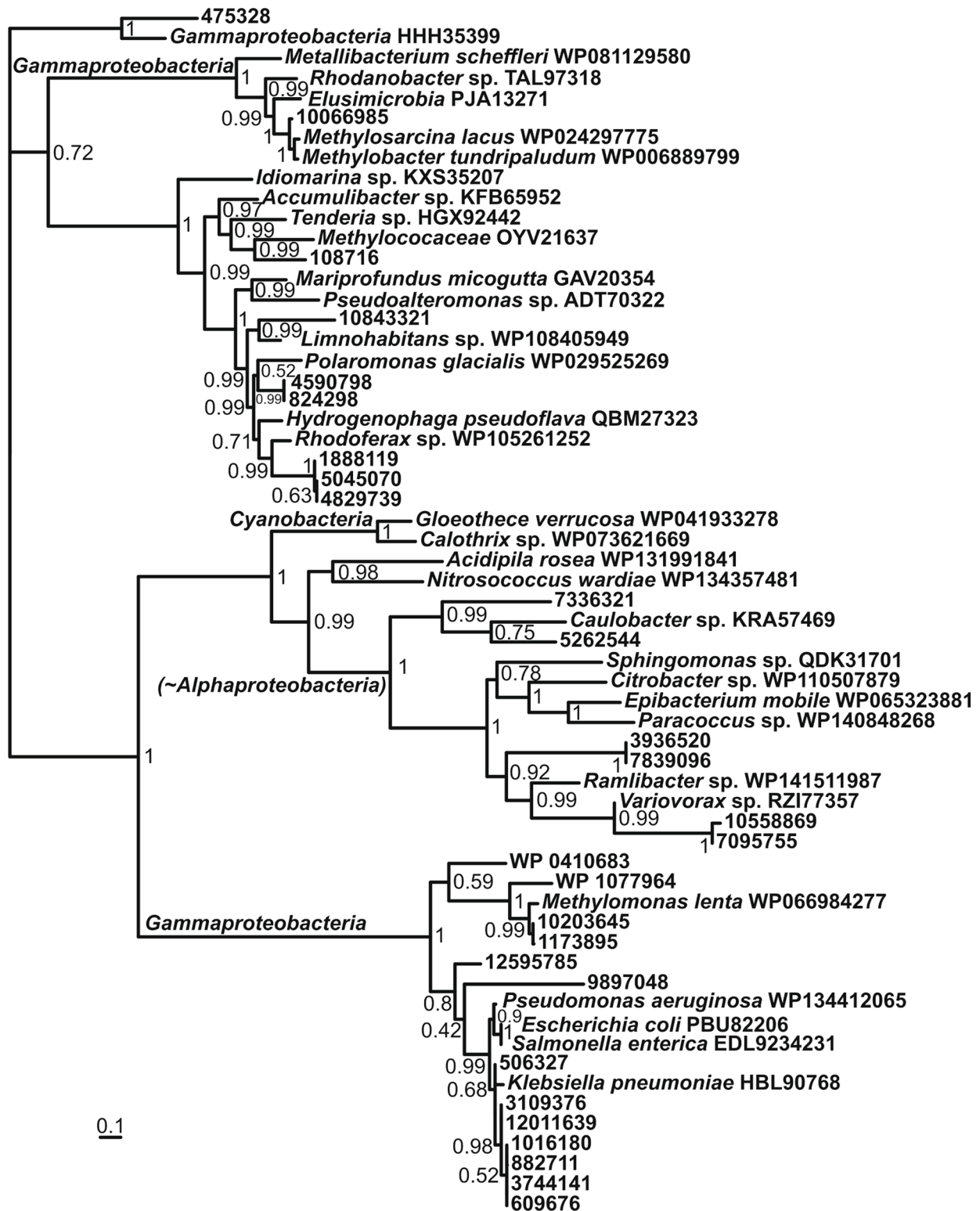
**Extended Data Fig. 1 | Generalised geological map of (a) Greenland and detailed geology of (b) the Kangerlussuaq region.** **a.** indicates the best interpretation of bedrock geology underlying the Greenland Ice Sheet from ref. <sup>82</sup> (lighter colours), with major geological provinces KMB (Ketilidian Mobile Belt), AB (Archaean Block), NMB (Nagssugtoqidian Mobile Belt), CM (Committee-Melville), EI (Ellesmere-Ingfield), V (Victoria), E (Ellesmerian) and CFB (Caledonian Fold Belt) indicated. Generalised oceanic currents are indicated by black arrows and derived from ref. <sup>83</sup>. **b.** displays more detailed geology of the Kangerlussuaq region where river sampling sites are located, and is derived from the GEUS Geological Map of Greenland<sup>75</sup>. The Precambrian shield bedrock underlying the study areas (Isunnguata Sermia, Russell Glacier, Leverett Glacier, NK and AF), covers > 75% of Greenland (orange and purple geologies; for example AB, NMB, KMB and CM).



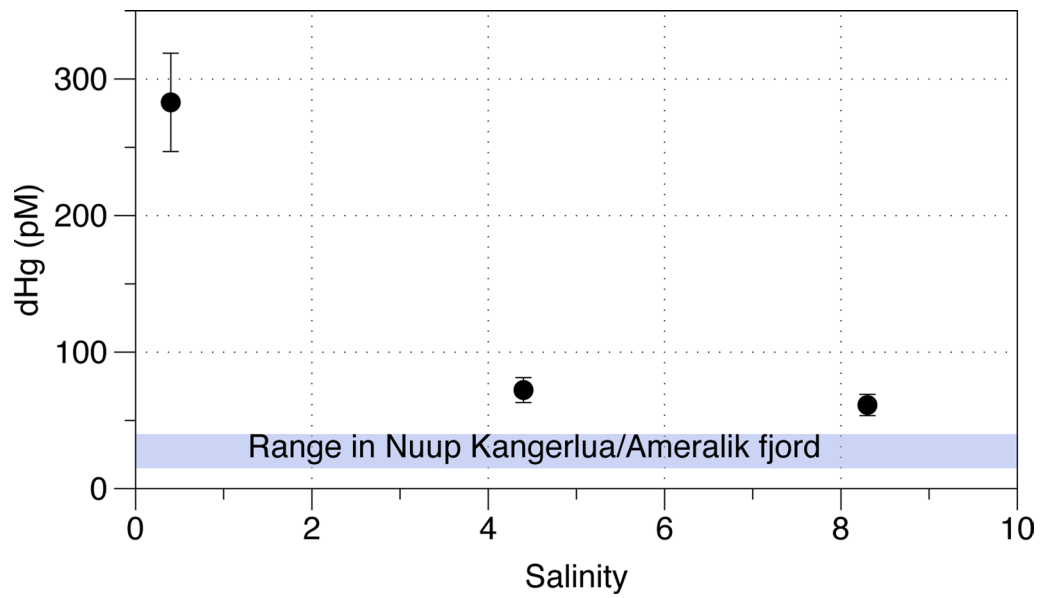
**Extended Data Fig. 2** | Dissolved organic carbon concentrations in the proglacial rivers of Leverett Glacier, Russell Glacier and Isunnguata Sermia.



**Extended Data Fig. 3 |** Southwestern region of the Greenland Ice Sheet used to estimate meltwater discharge fluxes in Table 1 with (a) ice sheet underlay and (b) geology underlay as per Fig. ED1. Study catchments areas are shown in the shaded region.

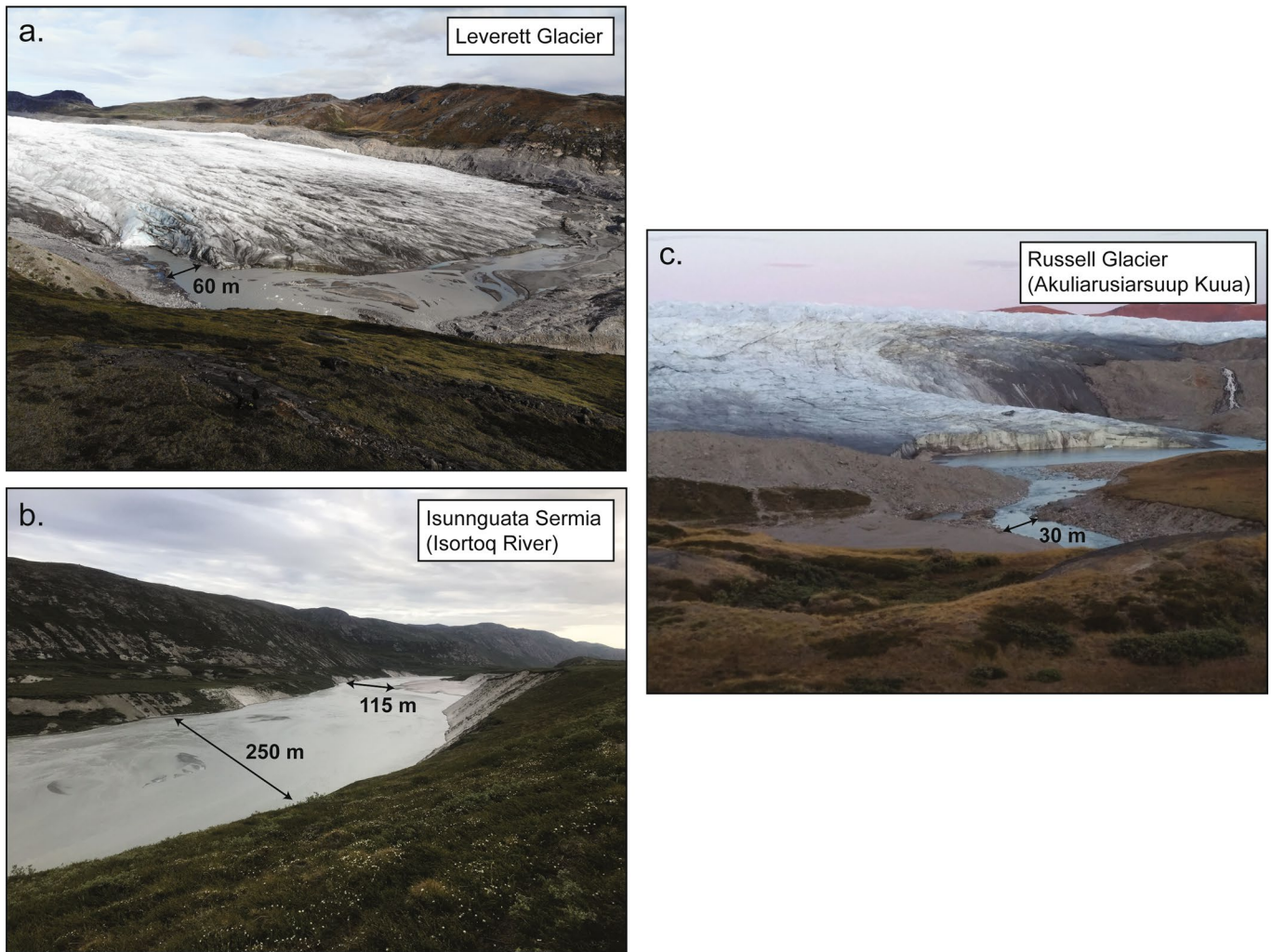


**Extended Data Fig. 4 |** Phylogenetic tree of microorganisms carrying the *merA* gene in subglacial meltwaters from Leverett Glacier. The sequences are taken from all four pooled samples (see Methods).



**Extended Data Fig. 5 | Total dissolved mercury concentrations from grab samples taken from surface waters at low salinities along Søndre Strømfjord (Fig. 1a) in 2012.** Uncertainty ( $\pm 12.7\%$ ) was calculated from replicate measurements of the low salinity sample. The range of concentrations from NK and Ameralik fjord are given in the shaded purple area (salinities of 17.0–32.4).














**Extended Data Fig. 6** | Images of glacial catchments/proglacial meltwater rivers sampled. (a) Leverett Glacier terminus, (b) Isortoq River (proglacial river of Isunnguata Sermia) looking upstream close to the sampling location in Fig. 1 and (c) Russell Glacier terminus (Akuliarusiarsuup Kuua) looking upstream. Approximate river widths are given for perspective.

## OPEN

## Author Correction: Large subglacial source of mercury from the southwestern margin of the Greenland Ice Sheet

Jon R. Hawkings , Benjamin S. Linhoff, Jemma L. Wadham, Marek Stibal , Carl H. Lamborg, Gregory T. Carling , Guillaume Lamarche-Gagnon , Tyler J. Kohler, Rachael Ward, Katharine R. Hendry , Lukáš Falteisek, Anne M. Kellerman, Karen A. Cameron , Jade E. Hatton, Sarah Tingey, Amy D. Holt, Petra Vinšová , Stefan Hofer , Marie Bulínová, Tomáš Větrovský, Lorenz Meire  and Robert G. M. Spencer

Correction to: *Nature Geoscience* <https://doi.org/10.1038/s41561-021-00753-w>, published online 24 May 2021.

In the version of this Article originally published online, the affiliation “US Geological Survey, Albuquerque, NM, USA” was mistakenly not listed as a present address; this has now been corrected and the other affiliations renumbered accordingly. All versions of the Article have been amended.



**Open Access** This article is licensed under a Creative Commons Attribution 4.0 International License, which permits use, sharing, adaptation, distribution and reproduction in any medium or format, as long as you give appropriate credit to the original author(s) and the source, provide a link to the Creative Commons license, and indicate if changes were made. The images or other third party material in this article are included in the article's Creative Commons license, unless

indicated otherwise in a credit line to the material. If material is not included in the article's Creative Commons license and your intended use is not permitted by statutory regulation or exceeds the permitted use, you will need to obtain permission directly from the copyright holder. To view a copy of this license, visit <http://creativecommons.org/licenses/by/4.0/>.

Published online: 30 June 2021

<https://doi.org/10.1038/s41561-021-00804-2>

© The Author(s) 2021

## Publisher Correction: Megathrusts exhumed

Correction to: *Nature Geoscience* <https://doi.org/10.1038/s41561-021-00757-6>, published online 7 May 2021.

In the version of this Editorial originally published, in the sentence beginning “An Article by Mallick et al.” the year of the earthquake was mistakenly given as ‘1868’ instead of ‘1861’; it has now been corrected in the online versions of the Editorial.

Published online: 4 June 2021

<https://doi.org/10.1038/s41561-021-00782-5>

© Springer Nature Limited 2021